Article:
Jiang, Q, Gao, Y, Wang, C et al. (11 more authors) (2017) Nitration of TRPM2 as a Molecular Switch Induces Autophagy during Brain Pericyte Injury. Antioxid Redox Signal, 27 (16). pp. 1297-1316. ISSN 1523-0864

https://doi.org/10.1089/ars.2016.6873

Original Research Communication

Nitration of TRPM2 as a Molecular Switch Induces Autophagy during Brain Pericyte Injury

Quan Jiang[1*], Yinping Gao[1,2*], Chengkun Wang[1], Rongrong Tao[1], Yan Wu[3], Kaiyu Zhan[3], Meihua Liao[1], Nannan Lu[1], Yingmei Lu[2], Christopher S Wilcox[4], Jianhong Linhua Jiang[5,6†], Wei Yang[3†], Feng Han[1†]

[1]Institute of Pharmacology and Toxicology, College of Pharmaceutical Sciences, Zhejiang University, Hangzhou, Zhejiang 310058, China;

[2]School of Medicine, Zhejiang University City College, Hangzhou, Zhejiang 310015, China;

[3]Department of Neurobiology, Key Laboratory of Medical Neurobiology, Innovation Center for Brain Science, Zhejiang University School of Medicine, Hangzhou, Zhejiang 310058, China;

[4]Hypertension, Kidney, and Vascular Research Center, Georgetown University Center, Washington, DC, USA;

[5]School of Biomedical Sciences, Faculty of Biological Sciences, University of Leeds, Leeds LS2 9JT, UK;

[6]Sino-UK Joint Laboratory of Brain Function and Injury, and Department of Physiology and Neurobiology, Xinxiang Medical University, Henan 453003, China

*These authors contributed equally to this work.

(1) Running title: Cross-talk between TRPM2 and autophagy

(2) †Correspondence to:

Dr. Feng Han, Institute of Pharmacology and Toxicology, Zhejiang University, 388 Yu-Hang-Tang Road, Hangzhou, 310058, China. Tel: 86-571-8820-8402; Fax: 86-571-8820-8402. E-mail: changhuahan@zju.edu.cn

Dr. Lin-Hua Jiang, School of Biomedical Sciences, Faculty of Biological Sciences, University of Leeds, Leeds LS2 9JT, UK. Tel: 44-113-3434231.

Email: l.h.jiang@leeds.ac.uk

Dr. Wei Yang, Department of Neurobiology, Zhejiang University School of Medicine, Hangzhou, China. Tel: 86-571-8820-8248; Fax: 86-571-8820-8248. E-mail: yangwei@zju.edu.cn

(3) 6078 words, 58 references, 10 figures, color illustration: 9, greyscale illustrations: 1, 17 supplementary figures, 0 tables.

Abstract

Aims: Dysfunction of neurovascular pericytes underlies breakdown of the blood-brain barrier, but the molecular mechanisms are largely unknown. In this study, we evaluated the role of the TRPM2 channel and autophagy during brain pericyte injury *in vitro* and *in vivo*. ***Results:*** A rapid induction in autophagy in human brain vascular pericytes, in zinc oxide nanoparticles (ZnO-NP)-induced cell stress model, was paralleled with an increase in the expression of the TRPM2-S truncated isoform, which was abolished by treatment with a nitric oxide synthase inhibitor and peroxynitrite scavenger. Furthermore, Y1485 in the C-terminus of the TRPM2 protein was identified as tyrosine nitration substrate by mass spectrometry. Overexpression of the Y1485S TRPM2 mutant reduced LC3-II accumulation and pericyte injury induced by ZnO-NP. Consistently, LC3-II accumulation was reduced and pericytes were better preserved in intact brain microvessels of the TRPM2 KO mice following ZnO-NP-induced vascular injury. ***Innovation and Conclusions:*** Our present study has revealed a novel mechanism of autophagy disturbance secondary to nitrosative stress-induced tyrosine nitration of TRPM2 during pericyte injury.

Introduction

The neurovascular pericytes are critical components of the blood-brain barrier (BBB) (27, 52, 54). Over the past decades, studies have concentrated mainly on the endothelial cell component. Recently, pericytes have gained increasing attention as important contributors to the maintenance of BBB function, vascular remodeling and reprogramming (21, 27, 40, 41, 52), and also as potential targets for therapies (40, 54). While the pericytes have been strongly implicated in regulating the permeability of the BBB and stress-induced pericyte injury (49), the precise underlying mechanisms remain elusive. Autophagy is a homeostatic cellular process that serves to control protein quality (36, 45). Recently, it has been reported that age-related pericyte degeneration might participate in cellular injury and trigger autophagic cell death (12). Accumulating evidence suggests that endoplasmic reticulum (ER) stress is a potent stimulus for autophagic response and develops prior to autophagy, as pharmacological inhibition of ER stress reduces autophagy (10, 31, 57). However, there have been conflicting reports regarding involvement of the ER stress-autophagy axis in inducing the pro-survival pathway or the pro-death pathway (6, 7, 34). It is important to note that the final outcome of the ER stress-autophagy axis highly depends on the strength and duration of stress-inducing signals. Therefore, it is necessary to examine the role of the ER stress-autophagy axis in particular cells under specific cellular contexts. It has been shown that zinc oxide nanoparticles (ZnO-NP)-induced toxicity leads to cell injury, which is a useful stress model to mimic the pathophysiological process of ER

stress and autophagy (3, 20, 39).

Recent findings have revealed that pericytes from brain microvessels strengthen the barrier integrity in primary cultures of rat brain endothelial cells (35). As a sensor of oxidative stress and mediator of Ca^{2+} entry and apoptosis, the transient receptor potential melastatin-related 2 (TRPM2) channels play a crucial role in a variety of physiological and pathological processes, such as regulating endothelial barrier function, increasing lung microvessel permeability and neutrophil sequestration (16, 25, 43, 51, 58). However, it is unclear how pericytes are damaged in response to stress stimulation and whether TRPM2 is involved in stress-induced pericyte injury.

The present study aimed to elucidate the molecular mechanism responsible for stress-induced pericyte injury. Using the ZnO-NP-induced stress model, in combination with genetic and pharmacological approaches, we investigated on the role of TRPM2 in the crosstalk that couple autophagy and microvascular pericyte injury. Our results from *in vitro* and *in vivo* studies provide compelling evidences to support a role for nitrosative stress in linking the TRPM2 turnover with disturbance of autophagy in brain pericyte injury.

Results

Spatiotemporal changes of autophagy in stress-induced brain pericyte injury

The autophagic process induced by ZnO-NP is an early event for the evaluation of cell injury (20, 39). The size distribution and zeta potential distribution of ZnO-NP were determined (Supplementary Fig. S1). We began with monitoring the temporal changes in the autophagy-lysosome signaling in cultured human brain vascular pericytes treated with ZnO-NP, using western blotting to detect membrane-bound LC3-II (the phosphatidylethanolamine-conjugated form). Treatment with ZnO-NP for 6 h induced a concentration-dependent increase in the LC3-II level (Fig. 1A and B).

Formation of the double-membrane cistern structures or autophagosomes containing cytoplasmic materials or aberrant organelles is an ultrastructural hallmark of autophagy (19, 36). Consistently with the biochemical data, transmission electron microscopy revealed the formation of double-membrane structures with engulfed cytoplasm fractions in pericytes after treatment with ZnO-NP for 6 h (Fig. 1C).

The accumulation of autophagosomes could indicate the dynamic process of autophagy (22). Therefore we next examined ZnO-NP-induced autophagy flux using fluorescence confocal microscopy in pericytes transfected with an mRFP-GFP-LC3 tandem construct, which is based on the concept of lysosomal quenching of GFP in GFP-labeled LC3(23, 33). As shown in Figure 1D, exposure to ZnO-NP for 6 h induced the formation of GFP-LC3 and mRFP-LC3 puncta, and an increase in

accumulation of yellow fluorescent puncta, which is indicative of autophagosome. Such effects were ZnO-NP concentration-dependent (Fig. 1D and E). These results were confirmed by immunofluorescence staining with the anti-LC3 antibody (Supplementary Fig. S2) to show an increase in autophagic vesicle accumulation in ZnO-NP-treated pericytes. Taken together, these results provide consistent evidence to indicate that autophagy initiation is increased following ZnO-NP-induced pericyte injury. Furthermore, time-lapse imaging showed that ZnO-NP induced dynamic changes in autophagy flux over a period of 60 min, as indicated by the fluorescence switch between GFP-LC3 puncta and mRFP-LC3 puncta (Fig. 1F, Supplementary Video 1). Autophagic flux can also be reflected by an elevation in the LC3-II level while interrupting the autophagosome-lysosome fusion step. As shown in Figure 1G, after inhibition of the lysosome function using bafilomycin A1 (50 nM), the LC3-II level in pericytes was further upregulated in response to ZnO-NP stimulation, suggesting increases in autophagy induction and autophagic flux (Fig. 1G and H, Supplementary Fig. S3).

TRPM2 knockdown blocks autophagy during brain pericyte injury

A recent study shows that the TRPM2 channel is important in mediating oxidative stress-induced disruption of lung endothelial barrier function (16). In the present study, we set out to investigate the role of TRPM2 during brain pericyte injury. The temporal changes in the TRPM2 expression in brain pericyte cells after injury

were examined using western blotting. Treatment with ZnO-NP induced a time-dependent increase in a protein band with a molecular weight of 95 kDa, expected for the short TRPM2 protein isoform (TRPM2-S) (Fig. 2A). The expression level of TRPM2-S relative to the full-length TRPM2 (TRPM2-L) was increased as the exposure was extended from 1 to 9 h (Fig. 2A and B). Therefore, our data indicate that ZnO-NP stimulation results in significant effect on the TRPM2 turnover in pericytes.

A recent study suggests TRPM2-S to be critically involved in reducing the HIF-1/2α level and mitophagy in SH-SY5Y neuroblastoma cells (4). We next investigated whether alteration in the TRPM2 protein expression affected the autophagy events in pericyte injury by examining the effect of reducing TRPM2 expression on LC3-II accumulation. Our results show that siRNA-mediated reduction in the TRPM2 expression significantly decreased LC3-II accumulation (Fig. 2C and D), indicating that ZnO-NP-induced LC3-II formation is TRPM2-dependent. Furthermore, we investigated whether ZnO-NP stimulation also disturbed autophagic flux in a TRPM2-dependent manner. After exposure to ZnO-NP for 2 h or 6 h, LC3-II accumulation was elevated further in pericytes treated with chloroquine (CQ, 25 μM) as compared with that in cells treated with CQ alone, indicating enhanced autophagic flux (Fig. 2E and F). Moreover, siRNA-mediated knockdown of the TRPM2 expression decreased LC3-II accumulation in pericytes in the absence and presence of CQ, indicating that TRPM2 participates in both autophagy induction and enhanced autophagic flux during pericyte injury (Fig. 2E and F).

TRPM2 knockdown reduces ER stress during brain pericyte injury

We next addressed the role of TRPM2 in ZnO-NP-induced brain pericyte injury using TUNEL staining. ZnO-NP treatment resulted in an increase in the percentage of TUNEL positive pericytes, which was almost completely abolished by treatment with TRPM2-siRNA (Fig. 3A and B), indicating TRPM2-dependent apoptotic cell death.

ER stress is a hallmark of cell injury, reflecting the extent of protein aggregation and promoting cell injury (48). The downstream ER stress markers, such as CHOP, JNK and PERK, are known to be involved in the ER stress-mediated autophagy and apoptosis pathway (42, 48). To further validate the observation that TRPM2 is involved in pericyte injury, we examined such ER stress signaling proteins. Indeed, exposure to ZnO-NP led to time-dependent up-regulation of CHOP, phospho-JNK (Thr183/Tyr185) and phospho-PERK (Thr981) in pericytes (Supplementary Fig. S4). Moreover, ZnO-NP-induced upregulation of ER stress-associated signaling activity in pericytes was significantly inhibited by treatment with TRPM2-siRNA (Fig. 3C-F).

To confirm that the observed TRPM2 turnover and ER stress-autophagy axis were causatively related to the severity of pericyte injury, ER stress-related signaling protein expression was examined. In contrast with the control cells, pericytes treated with ZnO-NP showed a significant increase in CHOP, phospho-JNK (Thr183/Tyr185) and phospho-PERK (Thr981) and again TRPM2 silencing decreased ZnO-NP-induced elevation in such ER stress signaling proteins in the presence of CQ (Fig. 3G, Supplementary Fig. S5). We further examined whether TRPM2 silencing

had a protective effect on the severe damage induced by prolonged exposure to ZnO-NP. Treatment with TRPM2-siRNA resulted in a significant protective effect in pericytes even after treatment with ZnO-NP for 24 h, as revealed by the downregulation of p-JNK and CHOP, along with the reduction in the degradation of IRE-1α and PERK (Fig. 3H). These results show that siRNA-mediated knockdown of the TRPM2 expression effectively reduces ZnO-NP-induced severe cell injury in pericytes.

We performed further experiments to determine whether autophagy events correlate with pericyte injury. As shown above, ZnO-NP treatment resulted in an increase in the percentage of TUNEL positive pericytes. In contrast, siRNA knockdown of ATG5 expression reduced the number of apoptotic cells (Fig. 4A and B), confirming that disturbance of autophagy promoted pericyte cell injury. Moreover, siRNA knockdown of ATG5 or TRPM2 significantly increased the cell viability and suppressed the activation of caspase-8 during brain pericyte injury (Fig. 4C-H).

Nitrosative stress associates with TRPM2-dependent autophagy

To better understand the molecular mechanisms underpinning TRPM2-dependent autophagy during pericyte injury, we examined the possible involvement of the nitrosative stress. It is known that peroxynitrite modifies tyrosine residues in proteins, which accounts for the effects of endogenously produced NO by oxidation and nitration reactions (14, 47). As shown in Figure 5A, western blotting analysis of

nitrotyrosine indicates that significant peroxynitrite formation was observed at 3 h after exposure to ZnO-NP and maintained throughout the treatment up to 12 h. To gain mechanistic insights, confocal imaging was used to detect the change in fluorescence intensity of NP3, an $ONOO^-$ probe in pericytes during treatment with ZnO-NP (Fig. 5B). There was significant increase in the NP3 fluorescence intensity in response to treatment with ZnO-NP, which was blunted by treatment with 200 μM uric acid, an $ONOO^-$ scavenger, prior to and during treatment with ZnO-NP (Fig. 5B). The autophagic flux can be morphologically traced with the mRFP-GFP-LC3 tandem construct. As shown above, the autophagic flux was increased following 6 h treatment with ZnO-NP. In contrast, treatment with uric acid led to barely discernible accumulations of yellow and red puncta upon during pericyte injury (Fig. 5C).

Of note, inhibition of nitric oxide synthase using N(G)-nitro-L-arginine methyl ester (L-NAME, 100 μM) was also capable of inhibiting ZnO-NP-induced elevation in the TRPM2-S expression in pericytes (Fig. 5D-F). Pretreatment of pericytes with uric acid alone or together with L-NAME led to similar results (Fig. 5D-F). Next, we assessed the functional relevance of $ONOO^-$ formation with autophagy signaling during pericyte injury. Exposure to ZnO-NP for 6 h led to 4~5-fold increases in ER signaling proteins (Fig. 5G-I). To elaborate our finding, the $ONOO^-$ was used to further clarify the role of nitrosative stress during pericyte injury. Treatment with $ONOO^-$ induced a pronounced increase in ER signaling proteins and excessive autophagy in pericytes (Supplementary Fig. S6). While a pronounced decrease in ER

signaling proteins (namely CHOP and phospho-JNK), and LC3-II was detected in ZnO-NP-exposed cells treated with L-NAME, uric acid or both (Fig. 5D-I), and in these cells, fewer apoptotic cells were observed by TUNEL staining (Supplementary Fig. S7). On the basis of these data, we conclude that there is a requirement for nitrosative stress signaling in engagement of the autophagy during pericyte injury.

In vitro nitration of TRPM2 protein

The TRPM2-L protein contains several tyrosine residues located in the C-terminal region. The assessment of TRPM2 nitration and identification of the nitration sites should provide critical information in unraveling the mechanisms of TRPM2-mediated autophagy and pericyte injury. To directly confirm that nitrosative stress was indeed responsible for protein tyrosine nitration of TRPM2, we treated a human TRPM2 peptide composed of a majority of the C-terminus (residues 1206-1504) with $ONOO^-$. Examination using MS/MS demonstrated that nitration caused a mass shift of +45 Da in 3-nitrotyrosine-containing peptides, and further identified that tyrosine nitration occurred at Y1485 residue (Fig. 6).

Mutation of the nitration site in the TRPM2 attenuates pericyte injury

To reinforce the crucial role of TRPM2 protein nitration in mediating pericyte injury, we mutated Y1485 to serine (Y1485S) and transfected pericytes with the plasmid encoding the TRPM2-Y1485S mutant protein (Fig. 7A). Western blotting revealed that CHOP and phospho-JNK were substantially higher in cells transfected

with the empty plasmid following 6 h exposure to ZnO-NP but not in cells transfected with TRPM2-Y1485S (Fig. 7B-F). In line with this, overexpression of the TRPM2-Y1485S mutant construct significantly attenuated excessive LC3-II formation during pericyte injury (Fig. 7B-F), as well as ER stress and autophagy in $ONOO^-$-treated pericytes (Fig. 7G-J). These results provide clear evidence to support that ZnO-NP-induced insult promotes activation of the ER stress-autophagy axis and pericyte injury and that these events are dependent of tyrosine nitration of TRPM2 at Y1485.

Nitrosative stress affects the TRPM2 channel function

We considered the possibility that tyrosine nitration of the TRPM2 protein regulated the TRPM2 channel function. To test this, ADP-ribose (ADPR)-induced TRPM2 channel currents were recorded in tetracycline-inducible TRPM2 expressing HEK293 cells (Fig. 8A). To examine whether the TRPM2 channel modulation could occur under nitrosative stress, we used SIN-1, a donor of $ONOO^-$ and a potent inducer of cell apoptosis as well as ZnO-NP. Treatment with SIN-1 and ZnO-NP resulted in significant decrease in ADPR-induced current amplitude (Fig. 8). The decrease induced by ZnO-NP or SIN-1 in the ADPR-induced current amplitude was prohibited by treatment with L-NAME or uric acid (Fig. 8A and B). Similar down-regulation by ZnO-NP or SIN-1 were observed for the wild-type TRPM2 channel but not the TRPM2-Y1485S mutant channel transiently expressed in HEK293 cells observed

(Supplementary Fig. S8). Taken together, these results suggest functional downregulation of the TRPM2 channels via nitration of tyrosine 1485.

Deletion of the TRPM2 reduces pericyte injury in mice

Pericytes are embedded within the basement membrane of microvessels (1, 12) and exhibit a number of characteristics for vessel maintenance and formation (52). To explore the pathophysiological significance of TRPM2-autophagy crosstalk identified from the *in vitro* studies described above, we extended our investigation to the brain pericytes *in vivo*. We examined pericyte injury in the cerebral vessels in the wild-type and age-matched TRPM2 KO mice following ZnO-NP injection, using immunofluorescent confocal imaging of α-SMA, one of the widely-accepted pericyte markers in brain microvessels (8) and laminin in the vascular-specific basal membrane (1). Pericytes were embedded within basement membranes with a continuous and patchy pattern in the capillaries. Double-labeling with α-SMA and laminin revealed more α-SMA-positive cells in the TRPM2 KO mice than in the wild-type mice following neurovascular insult (Fig. 9).

To provide further evidence to support the notion that excessive autophagy is associated with pericyte injury, adenovirus carrying mRFP-GFP-LC3 construct were injected into the mice brain to visualize the role of autophagy during ZnO-NP-induced pericyte injury. In addition to the weak fluorescence of LC3-GFP in the control mice, more mRFP-LC3 puncta were observed in the brain pericytes in the mice after

neurovascular insult (Fig. 10), indicating the increased autophagic process and flux activities. Moreover, the accumulation of autophagic vesicle was partially reduced in the vessels in the TRPM2 KO mice after neurovascular insult (Fig. 10). Therefore, the TRPM2 in pericytes has an important role in mediating excessive autophagy upon neurovascular insult.

Discussion

Pericytes dynamically respond to stress induced by injury in brain diseases. Recent studies provide compelling evidences that pericytes are essential for the preservation of the BBB function during ischemic stroke and Alzheimer's disease (40, 54). In this study, we have revealed a previously unrecognized role for the TRPM2 channel in promoting autophagy in pericytes and defined a novel mechanism of autophagy disturbance secondary to nitrosative stress-induced tyrosine nitration of TRPM2 protein during stress-induced pericyte injury.

In this study, we demonstrate that TRPM2-dependent autophagy is critically involved in the pathological process of pericyte injury. TRPM2 is a potentially important pharmacological target for inhibiting the pathological increase in endothelial barrier function (17). The importance of TRPM2 in mediating autophagy pericytes is supported by our finding that knockdown of TRPM2 partially inhibits ZnO-NP-induced LC3-II accumulation. Control experiments showed that TRPM2 knockdown did not significantly affect the LC3-II as well as ER stress protein levels during starvation (Supplementary Fig. S9). A recent study has reported that interference with TRPM2-L function modulates HIF-1/2α, mitochondrial function and mitophagy (4). Other studies have shown that overexpression of TRPM2-L confers protection against oxidative stress-induced cell death (5). A dramatic increase in the TRPM2-S was observed following pericyte injury. Zhang *et al* reported that TRPM2-S plays an important role in many tissues because it can modulate Ca^{2+} influx

and cellular responses to oxidative stress (56). Recently, Hecquet *et al* have shown that TRPM2-S expression during oxidative stress may mitigate endothelial cell apoptosis and vascular injury and inflammation (17, 18).

To search for a link between TRPM2-dependent autophagy and pericyte injury, we investigated if TRPM2 or autophagy inhibition can affect cell survival after subjected to ZnO-NP-induced insult. Here, we showed that either downregulation of endogenous TRPM2 expression in pericytes by siRNA *in vitro* or TRPM2 knockout in mice consistently reduced LC3-II accumulation and pericyte injury. Of particular note, we found that siRNA knockdown of ATG5 markedly attenuated pericyte apoptosis, indicating that autophagy serves as an important cell death mechanism. In this study, we also demonstrated that autophagy during pericyte injury strongly depends on ER stress, which was confirmed by the finding that treatment with salubrinal, a selective inhibitor of ER stress significantly blocked ZnO-NP-induced LC3II formation (Supplementary Fig. S10). Moreover, siRNA-mediated knockdown of TRPM2 significantly blunted tunicamycin-induced ER stress and LC3II formation in pericytes (Supplementary Fig. S11). In addition, our data showed that autophagy and ER-stress signaling were Ca^{2+}-dependent and inhibited by a TRPM2 blocker (Supplementary Fig. S12). Thus, our data suggest that autophagy changes as a regulator of pericyte injury, TRPM2 lies upstream of the ER stress-autophagy axis and autophagy is functioning primarily as a cytotoxic response to excess ER stress.

How does stress stimulation induce TRPM2-dependent autophagy and

subsequently pericyte injury? We have further explored the upstream regulation of TRPM2 channel function underlying pericyte injury. The present study demonstrated that nitrosative stress is an important element in the induction of TRPM2 turnover and the autophagy response. We previously reported that Ca^{2+}/calmodulin-dependent nitrosative stress initiated early cerebrovascular injury and subsequent neuronal damage, indicating that brain microvessels are the most vulnerable and sensitive cellular components of $ONOO^-$ (13, 46, 48). In the present study, the Ca^{2+} sensor protein calmodulin was identified as one of the TRPM2-interacting proteins using a proteomic approach. Immunoprecipitation confirmed that TRPM2 and calmodulin associate, whereas this association was decreased in the presence of ZnO-NP (Supplementary Fig. S13). We hypothesize that ongoing nitrosative stress induces the TRPM2 turnover, and subsequently induces ER stress to initiate the autophagy pathway. The above process is, at least in part, dependent on nitration of TRPM2 at Y1485. TRPM2 nitration does not directly trigger autophagy and instead activates ER stress that provides the critical link to the increased autophagy. In the present study, overexpression of the TRPM2 Y1485S construct significantly reduced the LC3II formation in tunicamycin-treated pericytes (Supplementary Fig. S14). The autophagy induced by the TRPM2 turnover is likely through ER signaling and the consequent cascade of reactions related to the unfolded protein response (15, 24, 38). Our data suggested that nitration of TRPM2 at Y1485 might contributes to TRPM2-S formation because both the NOS inhibitor (L-NAME) and peroxynitrite scavenger

(uric acid) significantly reduced TRPM2-S formation and restored the TRPM2-L channel function. These results further support the notion that a nitrosative stress-dependent mechanism might regulate the TRPM2 turnover during pericyte injury. These steps were in parallel with an inhibition of CHOP and phospho-JNK (Thr183/Tyr185), and an increase in the level of LC3-II in the same context.

The neurovascular unit is the primary target of nitrosative stress in cardiovascular diseases, stroke, and neurodegenerative disorders (2, 46, 47). The toxicity of superoxide is greatly increased by reacting with nitric oxide to form peroxynitrite (44, 47). Here, combined treatments with L-NAME and uric acid did not further reduce anti-nitrosative stress efficacy following ZnO-NP insult, indicating that the nitrosative stress pathway is specifically involved in the pathological process of pericyte injury. Further support for this conclusion is provided by the observation that overexpression of the TRPM2-Y1485S mutant was sufficient to inhibit the ER stress, coinciding with the inhibitory effect on the elevation of LC3-II accumulation during pericyte injury. Our results together with these observations suggest that inhibition of TRPM2 protein tyrosine nitration protects against pericyte injury via inhibition of autophagy.

A number of studies demonstrate that pericyte-endothelial cell communication is essential to regulate the capillary blood flow and maintain the function of the BBB (9, 11, 37). Indeed, pericytes are a key component of the neurovascular unit, which wrap around the endothelial cells in the microvessels, eliciting a protective effect on

endothelial barrier function (9, 16). To assess the translational relevance *in vivo*, we addressed the role of pericyte TRPM2 channel during ZnO-NP-induced neurovascular injury. Interestingly, the decreased abundance of pericyte LC3 puncta at 24 h after neurovascular injury in the TRPM2 KO mice coincided with reduced pericyte injury in brain microvessels. Taken together, these genetic and biochemical results support the idea that TRPM2-dependent autophagy plays a crucial role in mediating nitrosative stress-induced pericyte injury in mice. Moreover, our study also raises interesting questions regarding the interrelationships between pericyte-specific TRPM2 channels and other neurovascular components in the pathological process of neurovascular injury. However, this hypothesis remains to be tested in the future.

In summary, our study has established a previously unrecognized mechanism for nitrosative stress-induced TRPM2 protein tyrosine nitration and subsequent disturbance of autophagy leading to pericyte injury. More importantly, our results provide clues for developing more effective neurovascular therapeutic strategies by targeting nitrosative stress. Ultimately, a full understanding of the molecular mechanisms of pericyte injury is crucial to the development of therapeutic strategies to treat neurovascular dysfunction-related pathologies.

Innovation

Our study is the first demonstration that TRPM2-dependent autophagy is critically involved in the pathological process of pericyte injury. Our findings further have identified nitrosative stress as an important element in the induction of TRPM2 tyrosine nitration at Y1485 and the autophagy response. Mutational prevention of this significantly reduced the elevation of ER apoptotic proteins and LC3-II accumulation during pericyte injury. LC3 accumulation was reduced and brain pericytes were better preserved in the TRPM2 KO mice upon vascular injury. A full understanding of the molecular mechanisms of pericyte injury is crucial to the development of therapeutic strategies to treat neurovascular dysfunction-related pathologies.

Materials and Methods

Reagents

All chemicals were purchased from Sigma-Aldrich (St. Louis, MO, USA) unless otherwise specified.

Characterization of the size, morphology and zeta potential for zinc oxide nanoparticles

Zinc oxide nanoparticles (Sigma, 721077) suspension stock was prepared in phosphate buffer saline (PBS) at 10 mg/ml and treated with ultrasound to make uniform distribution. The particles size and zeta potential distribution were determined with a Zetasizer (3000HS, Malvern Instruments, UK) after the prepared dispersion performed 100-fold dilutions with distilled water. The particle size and surface morphologies were further characterized using a transmission electronic microscope (JEM-1230, JEOL, Japan). The samples were placed on copper grids for viewing.

Culture of human brain pericytes

Human brain vascular pericytes (#1200) were purchased from ScienCell Research Laboratories (Carlsbad, CA, USA) and cultured in pericyte growth medium (contains growth factors, hormones and proteins, ScienCell Research Laboratories, Catalog #1252) in a humidified atmosphere containing 5% CO_2 at 37°C. Cells between

passages 3 and 7 were used in this study.

Treatment of human pericytes with ZnO-NP

Human pericytes were plated in six-well plates at a density of 2×10^6 cells per well in a final volume of 2 mL. An appropriate aliquot of ZnO-NP was added to achieve a desired concentration. L-NAME (100 μM) or chloroquine (25 μM) was added into the well with ZnO-NP (10 μg/ml) at the same time and the cells were incubated for 6 h. Uric acid (200 μM) was added 3 h prior to addition of ZnO-NP (10 μg/ml). Cells treated with indicated concentrations of ZnO-NP for 6 h were used for western blotting or immunocytochemistry, and cells that were not exposed to ZnO-NP were used as control.

RNA interference

Human pericytes were cultured in 6-well plates in growth medium. Transfection with either double-stranded siRNA targeting TRPM2, ATG5 or a control scramble siRNA using Lipofectamine RNAiMAX (Invitrogen, 13778075) was conducted according to the manufacturer's instructions. siRNA of TRPM2 (sense: 5'-UGAUCCAGCAGAAACUGAGCGUGUU-3' and anti-sense: 5'-AACACGCUCAGUUUCUGCUGGAUCA-3') and control scramble siRNA were purchased from Thermo Fisher Scientific. siRNA of ATG5 (sc-41445) were purchased from Santa Cruz Biotechnology. The gene-silencing efficacy of siRNA are depicted in supplementary Figure S15.

Mice

The TRPM2 KO mice were generated in the C57BL/6 background as detailed in our previous studies (53, 58). Both wild-type (C57BL/6 strain) and TRPM2 KO mice were housed under standard conditions with a 12/12 h light/dark cycle and free access to food and water. 8 to 12-week-old male mice weighing 22–25 g were used in the study and were randomly assigned to each group. All animal use procedures were approved by the Committees at Zhejiang University and Leeds University for the Care and Use of Laboratory Animals. All the experiments were performed at room temperature or specifically indicated.

CCK-8 assays

A Cell Counting Kit-8 (CCK-8) assay (Dojindo, CK04) was used to measure cell viability. Human pericytes were seeded in 96-well plates at a density of 2.5×10^3 cells per well and incubated overnight to allow for cells to settle down, before being transfected with siRNA-ATG5 or negative control for 48 h. Furthermore, the culture medium was changed to 100 μl fresh medium containing ZnO-NP (10 μg/ml) with or without Z-VAD-FMK (a caspase inhibitor, 10 μM) and incubated for further 6 h. Cells in each well were incubated for one hour with 110 μl fresh medium containing 10 μl CCK-8 reagent. Finally, the cell viability was determined by measuring the optical absorbance at 450 nm using a multimode reader (Beckman Coulter, DTX880).

Injection of ZnO-NP in mice

The procedures were approved by the Committee on Animal Experiments at Zhejiang University, and conformed to the Guide for the Care and Use of Laboratory Animals published by the US National Institutes of Health (NIH Publication No. 85-23, revised 1996). The male mice were injected with 0.1 mL of 0.5 mg/ml ZnO-NP via the tail vein. The control mice were injected with a same volume of vehicle. For immunohistochemical analysis, mice were anesthetised through diethyl ether inhalation in a chamber 24 h post-injection, and their brains were removed for analysis.

Injection of adenovirus vector carrying mRFP-GFP-LC3 in mice

Adenovirus vector carrying mRFP-GFP-LC3 construct (Hanbio Biotechnology, Shanghai, China) was injected into the bilateral ventricle over a 10-min duration using a Hamilton microsyringe with the coordinates of 0.5 mm caudal to the bregma, 1 mm lateral to the midline, and 3 mm depth from the skull surface under the guidance of a stereotaxic instrument. Two weeks following injection, the male mice were injected with 0.1 mL of 0.5 mg/ml ZnO-NP *via* the tail vein. The adenovirus batches used for experiments had comparable titres ranging from 1×10^{10} to 1×10^{11} integration units/ml. Virus suspensions were stored at -80°C until use and were briefly centrifuged and kept on ice immediately before injection.

Western blotting

Western blotting was carried out by SDS polyacrylamide gel electrophoresis

(SDS-PAGE) as described previously (48). Briefly, cells were homogenized in the homogenizing buffer containing 50 mM Tris-HCl (pH 7.4), 0.5% Triton X-100, 4 mM EGTA, 10 mM EDTA, 1 mM Na_3VO_4, 30 mM sodium pyrophosphate, 50 mM NaF, 100 nM calyculin A, 50 μg/ml leupeptin, 25 μg/ml pepstatin A, 50 μg/ml trypsin inhibitor and 1 mmol/L dithiothreitol. For TRPM2 detection, membrane fractionation from cell lysates was performed as we previously described (29). The following primary antibodies were used: nitrotyrosine (1:1000, Merck Millipore, 05-233), TRPM2 (1:1000Abcam, ab11168), LC3 (1:5000, Sigma Aldrich, L7543), Phospho-SAPK/JNK(Thr183/Tyr185) (1:2000, Cell Signaling Technology, 4668), JNK (1:2000Santa Cruz Biotechnology, sc-571), IRE1α (1:1000, Cell Signaling Technology, 3294), Phospho-PERK (Thr981) (1:1000, Santa Cruz Biotechnology, sc-32577), PERK (1:1000, Cell Signaling Technology, 5683), CHOP (1:500, Cell Signaling Technology, 5554), caspase 8 (1:1000, active form, Biovision, 3258), caveolin-1 (1:5000, Cell Signaling Technology, 32667) and β-actin (1:5000, Sigma Aldrich, A5441). Protein intensities were analyzed by Image J software (NIH), and normalized against the β-actin or caveolin-1 band in the matched experiments. For immunoprecipitation, cells were lysed in the lysis buffer (10 mM Tris-HCl, pH7.5, 0.5% NP-40, 150 mM NaCl, 1 mM EDTA) supplemented with a complete protease inhibitor cocktail (Roche). Cell lysates were incubated with 2 μg of indicated antibodies for overnight at 4°C, followed by incubation at 4°C with protein A/G-agarose beads for 4 h. Immunoprecipitated samples were washed six times with

lysis buffer, electrophoresed on SDS-PAGE, and subjected to Western blot analysis as described above. All full unedited blot are displayed in Supplementary Fig. S16.

Transmission electron microscopy

The ultrastructures of human pericytes was determined using transmission electron microscopy. Cells were washed twice with PBS and fixed in 2.5% glutaraldehyde in PBS (pH 7.4). The fixed cells were detached by gentle scraping, pelleted, fixed in 1% osmium tetroxide and imaged using a Philips Tecnai 10 transmission electron microscope (Philips, Holland).

Immunofluorescence confocal microscopy

Immunolocalization and changes in LC3 in pericytes were examined by confocal microscopy. Briefly, after indicated treatment, cells seeded on coverslips were washed 3 times in PBS and fixed in 4% formaldehyde. To quantify LC3-positive vesicles, cells were transfected with mRFP-GFP-LC3 plasmid or were fixed and stained with anti-LC3 antibody (Cell Signaling Technology, 2775). Images were acquired using a Nikon A1R confocal microscope with a ×60 oil immersion lens at 1024×1024 pixel resolution. The average number of GFP- or mRFP-LC3 puncta per cell was determined by using an Imaris Imaging Software (Bitplane) (50). For time-lapse confocal imaging of live cells, after transfected with mRFP-GFP-LC3 plasmid, human pericytes were cultured on glass-bottomed dishes overnight, and incubated with or without ZnO-NP (15 μg/ml). The changes in GFP and mRFP fluorescence intensity

were captured by Olympus IX-81 confocal microscope for 120 min which equipped with a ×60 oil-immersion lens, a polychrome IV light source (Till Photonics), a 505 DCXR beam splitter, and a CCD camera (ANDOR iXon3).

To immunolabel the mouse brain sections, slices were incubated with antibodies against LC3 (1:200, Cell Signaling Technology, 2775), alph-smooth muscle actin (1:250, Abcam, ab7817) and laminin (1:200, Abcam, ab11575) overnight at 4°C. After washing, the slices were incubated with Alexa fluor 488-conjugated anti-rabbit IgG (Invitrogen, A-21206) and/or Alexa fluor 594-conjugated anti-mouse IgG (Invitrogen, A-21203) in Tris-NaCl-blocking buffer (1:400). NP3, a fluorescent switch-on probe was used to examine the $ONOO^-$ formation, as previously reported (26). To minimize nonspecific staining, the experiments include a negative control using the IgG with no primary antibody (Supplementary Fig. S17). Immunofluorescence was captured using a Zeiss LSM 510 confocal microscope. The number of the disconnected patchy parts were analyzed by Imaris Imaging Software (Bitplane). The 3D filled plots were processed by using ImageJ v1.45 with the accompanied 'Interactive 3D Surface Plot' plug-in.

TUNEL assay

Apoptotic cell death was assessed using a terminal deoxynucleotidyl transferase dUTP nick end labeling (TUNEL) staining (30, 48). Images were recorded after counterstaining with DAPI, and pericytes were identified by phase image. Five

random fields were examined on each coverslip, and the experiments were repeated 4 times. Apoptotic cell death was presented as the percentage of $TUNEL^+$ cells in the total number of cells identified by DPAI staining. In addition, the caspase 8 activity assay kit (Abcam, ab39700) were also used to study the effect of siRNA mediated knockdown of Atg5 or TRPM2 expression on cell death. Collected the cell samples with indicated conditions and suspended cells in 50 μL of ice cold cell lysis buffer provided by assay kit. Incubated with reaction buffer and IETD-*p*NA substrate after transfer the supernatant. Detected on a microplate reader (Beckman Coulter, DTX880) at OD 405 nm as described in instructions.

Propidium iodide flow cytometry analysis

Flow cytometric assays to evaluate cell death by propidium iodide (PI) (Sigma-Aldrich, P4170) staining were performed essentially as previously described, following the manufacturer's instructions. Briefly, human pericyte cells, after treated with indicated conditions, were incubated in solutions containing (50 μg/ml PI, 100 μg/ml RNase A, 0.2% Triton X-100) at room temperature for 30 min in the dark. At least 1×10^4 cells were analyzed for each sample using a FACS-Calibur flow cytometer (BD Biosciences)

In vitro protein nitration of TRPM2 and mass spectrometry analysis

A 10 μg portion of recombinant TRPM2 was reacted with 100 μM $ONOO^-$ for 1 h in 50 mM phosphate buffer (pH 7.4) containing 0.1% Lauryl-β-D-maltoside (28, 46).

The mixture was treated with 9% of ethanol at 40°C for 10 min and centrifuged at 75,600 *g* for 30 min. The $ONOO^-$-treated TRPM2 (10 μg/lane) was subjected to SDS-PAGE and silver staining. The protein band with a size corresponding to that of the recombinant TRPM2 peptide was excised and further prepared for mass spectrometry analysis. Sequence information from the MS/MS data was processed using the Mascot 2.0 active perl script with standard data processing parameters (28, 46). Database was searched with MASCOT 2.0 (Matrix Science, Boston, MA). As compared to the protein untreated with $ONOO^-$, a nitrated peptide was determined by a mass shift of +45 Da to the corresponding y and b ions.

Site-directed mutagenesis, plasmid constructs and transfection

PCR-based site-directed mutagenesis was performed as detailed previously (58). In brief, the full-length human TRPM2 sequence with C-terminal Glu-Glu tag in pcDNA3.1 vector was used as a DNA template (32). The forward and reverse primers used were 5'-AGG CGC ATC CCA CTC TCT GCG AAC CAC AAG ACC-3' and 5'-GGT CTT GT GGT TCG CAG AGA GTG GGA TGC GCC3', respectively. The mutation was confirmed by sequencing.

Human pericytes cultured in six-well plates in growth medium were transfected with plasmid encoding the wild-type and Y1485S mutant TRPM2 protein, or an empty plasmid as control using Lipofectamine 3000 (Invitrogen, L3000-015) (Supplementary Fig. S18 A and B). The transfection medium was replaced with fresh

growth medium 6 h later, and the cells were collected for experiments 2 days after transfection. For electrophysiological study shown in Supplementary Figure S8, the wild-type and Y1485S mutant TRPM2 channels were transiently expressed in HEK293 cells as described in our previous study (55).

Whole-cell patch clamp recording

Whole-cell patch-clamp recordings were performed using Axonpatch 200B amplifier as previously described, from tetracycline-inducible HEK293 cells stably expressing human TRPM2 (hTRPM2) channel, induced with 1 μg/ml tetracycline for 12-24 h, and also from HEK293 cells transiently transfected with the wild type or Y1485S mutant human TRPM2 channel (Supplementary Fig. S18 C and D). Before recording, cells were exposed to ZnO-NP (10 μg/ml) with or without 3-morpholinosydnonimine (SIN-1, 0.5 mM), L-NAME (100 μM) and uric acid (UA, 200 μM). Change of the extracellular solutions was performed by using a RSC-160 system (Biologic Science Instruments). The membrane potential was held at 0 mV. Voltage ramps with 500-ms duration from -100 mV to 100 mV were applied every 5 s. Data were acquired at 10 kHz and filtered offline at 50 Hz. For analysis, the mean of the first three ramps before channel activation was used for leak-subtraction of all subsequent current records.

Statistical analysis

Results are shown as mean ± S.E.M., where appropriately. For all Western-blot,

immunohistochemistry, cell viability assay and patch clamp recording experiments unless otherwise specified below, one-way ANOVA followed by Tukey's *post hoc* test were used for comparisons among three or more groups. For TUNEL assay and other experiments, unpaired two-tailed Student's *t*-test was used for comparisons between two groups. Statistical analyses were carried out using GraphPad Prism 6 (GraphPad Software). And $P < 0.05$ was considered to be statistically significant.

Acknowledgments

This work was supported in part by National Natural Science Foundations of China (81120108023, 81573411, 81473202, 31471118); National Basic Research Program of China (2013CB910204, 2014CB910300); The Zhejiang Province Program for Cultivation of High-level Health Talents and New Century 151 Talent Project of Zhejiang Province; Department of Education, Henan Province and University of Leeds-Zhejiang University Strategic Collaboration Partnership Programmer.

Author Disclosure Statement

No potential conflicts of interest were disclosed.

List of Abbreviations

Baf-A1, Bafilomycin A1

BBB, blood-brain barrier

CaM, Calmodulin

CQ, chloroquine

DAPI, 4',6-diamidino-2-phenylindole dihydrochloride

ER, endoplasmic reticulum

LC3, microtubule-associated protein 1 light chain 3

PBS, phosphate buffer solution

RNS, reactive nitrogen species

SDS-PAGE, sodium dodecyl sulfate polyacrylamide gel electrophoresis

siRNA, small interference RNA

TEM, transmission electron microscopy

TRPM2, transient receptor potential melastatin-related 2

PI, propidium iodide

References:

1. Armulik A, Genove G and Betsholtz C. Pericytes: developmental, physiological, and pathological perspectives, problems, and promises. *DEV CELL* 21: 193-215, 2011.
2. Calabrese V, Sultana R, Scapagnini G, Guagliano E, Sapienza M, Bella R, Kanski J, Pennisi G, Mancuso C, Stella AM, and Butterfield DA. Nitrosative stress, cellular stress response, and thiol homeostasis in patients with Alzheimer's disease. *Antioxid Redox Signal* 8: 1975-1986, 2006.
3. Chen R, Huo L, Shi X, Bai R, Zhang Z, Zhao Y, Chang Y, and Chen C. Endoplasmic reticulum stress induced by zinc oxide nanoparticles is an earlier biomarker for nanotoxicological evaluation. *ACS NANO* 8: 2562-2574, 2014.
4. Chen SJ, Hoffman NE, Shanmughapriya S, Bao L, Keefer K, Conrad K, Merali S, Takahashi Y, Abraham T, Hirschler-Laszkiewicz I, Wang J, Zhang XQ, Song J, Barrero C, Shi Y, Kawasawa YI, Bayerl M, Sun T, Barbour M, Wang HG, Madesh M, Cheung JY, and Miller BA. A splice variant of the human ion channel TRPM2 modulates neuroblastoma tumor growth through hypoxia-inducible factor (HIF)-1/2alpha. *J BIOL CHEM* 289: 36284-36302, 2014.
5. Chen SJ, Zhang W, Tong Q, Conrad K, Hirschler-Laszkiewicz I, Bayerl M, Kim JK, Cheung JY, and Miller BA. Role of TRPM2 in cell proliferation and susceptibility to oxidative stress. *Am J Physiol Cell Physiol* 304: C548-C560, 2013.
6. Ciechomska IA and Kaminska B. ER stress and autophagy contribute to CsA-induced death of malignant glioma cells. *AUTOPHAGY* 8: 1526-1528, 2012.
7. Deegan S, Saveljeva S, Logue SE, Pakos-Zebrucka K, Gupta S, Vandenabeele P, Bertrand MJ, and Samali A. Deficiency in the mitochondrial apoptotic pathway reveals the toxic potential of autophagy under ER stress conditions. *AUTOPHAGY* 10: 1921-1936, 2014.
8. Dore-Duffy P, Wang S, Mehedi A, Katyshev V, Cleary K, Tapper A, Reynolds C, Ding Y, Zhan P, Rafols J, and Kreipke CW. Pericyte-mediated vasoconstriction underlies TBI-induced hypoperfusion. *NEUROL RES* 33: 176-186, 2011.
9. Fisher M. Pericyte signaling in the neurovascular unit. *STROKE* 40: S13-S15, 2009.
10. Fouillet A, Levet C, Virgone A, Robin M, Dourlen P, Rieusset J, Belaidi E, Ovize M, Touret M, Nataf S, and Mollereau B. ER stress inhibits neuronal death by promoting autophagy. *AUTOPHAGY* 8: 915-926, 2012.
11. Goritz C, Dias DO, Tomilin N, Barbacid M, Shupliakov O, and Frisen J. A pericyte origin of spinal cord scar tissue. *SCIENCE* 333: 238-242, 2011.
12. Gu X, Liu XY, Fagan A, Gonzalez-Toledo ME, and Zhao LR. Ultrastructural changes in cerebral capillary pericytes in aged Notch3 mutant transgenic mice. *ULTRASTRUCT PATHOL* 36: 48-55, 2012.

13. Han F, Chen YX, Lu YM, Huang JY, Zhang GS, Tao RR, Ji YL, Liao MH, Fukunaga K, and Qin ZH. Regulation of the ischemia-induced autophagy-lysosome processes by nitrosative stress in endothelial cells. *J PINEAL RES* 51: 124-135, 2011.
14. Han F, Shirasaki Y and Fukunaga K. Microsphere embolism-induced endothelial nitric oxide synthase expression mediates disruption of the blood-brain barrier in rat brain. *J NEUROCHEM* 99: 97-106, 2006.
15. Hart LS, Cunningham JT, Datta T, Dey S, Tameire F, Lehman SL, Qiu B, Zhang H, Cerniglia G, Bi M, Li Y, Gao Y, Liu H, Li C, Maity A, Thomas-Tikhonenko A, Perl AE, Koong A, Fuchs SY, Diehl JA, Mills IG, Ruggero D, and Koumenis C. ER stress-mediated autophagy promotes Myc-dependent transformation and tumor growth. *J CLIN INVEST* 122: 4621-4634, 2012.
16. Hecquet CM, Ahmmed GU and Malik AB. TRPM2 channel regulates endothelial barrier function. *ADV EXP MED BIOL* 661: 155-167, 2010.
17. Hecquet CM, Ahmmed GU, Vogel SM, and Malik AB. Role of TRPM2 channel in mediating H2O2-induced Ca2+ entry and endothelial hyperpermeability. *CIRC RES* 102: 347-355, 2008.
18. Hecquet CM, Zhang M, Mittal M, Vogel SM, Di A, Gao X, Bonini MG, and Malik AB. Cooperative interaction of trp melastatin channel transient receptor potential (TRPM2) with its splice variant TRPM2 short variant is essential for endothelial cell apoptosis. *CIRC RES* 114: 469-479, 2014.
19. Jiang P and Mizushima N. Autophagy and human diseases. *CELL RES* 24: 69-79, 2014.
20. Johnson BM, Fraietta JA, Gracias DT, Hope JL, Stairiker CJ, Patel PR, Mueller YM, McHugh MD, Jablonowski LJ, Wheatley MA, and Katsikis PD. Acute exposure to ZnO nanoparticles induces autophagic immune cell death. *NANOTOXICOLOGY* 9: 737-748, 2015.
21. Karow M, Sanchez R, Schichor C, Masserdotti G, Ortega F, Heinrich C, Gascon S, Khan MA, Lie DC, Dellavalle A, Cossu G, Goldbrunner R, Gotz M, and Berninger B. Reprogramming of pericyte-derived cells of the adult human brain into induced neuronal cells. *CELL STEM CELL* 11: 471-476, 2012.
22. Klionsky DJ, Abdelmohsen K, Abe A, Abedin MJ, Abeliovich H, Acevedo AA, Adachi H, Adams CM, Adams PD, Adeli K, Adhihetty PJ, Adler SG, Agam G, Agarwal R, Aghi MK, Agnello M, Agostinis P, Aguilar PV, Aguirre-Ghiso J, Airoldi EM, Ait-Si-Ali S, Akematsu T, Akporiaye ET, Al-Rubeai M, Albaiceta GM, Albanese C, Albani D, Albert ML, Aldudo J, Algul H, Alirezaei M, Alloza I, Almasan A, Almonte-Beceril M, Alnemri ES, Alonso C, Altan-Bonnet N, Altieri DC, Alvarez S, Alvarez-Erviti L, Alves S, Amadoro G, Amano A, Amantini C, Ambrosio S, Amelio I, Amer AO, Amessou M, Amon A, An Z, Anania FA, Andersen SU, Andley UP, Andreadi CK, Andrieu-Abadie N, Anel A, Ann DK, Anoopkumar-Dukie S, Antonioli M, Aoki H, Apostolova N, Aquila S, Aquilano K, Araki K, Arama E, Aranda A, Araya J, Arcaro A, Arias E, Arimoto

H, Ariosa AR, Armstrong JL, Arnould T, Arsov I, Asanuma K, Askanas V, Asselin E, Atarashi R, Atherton SS, Atkin JD, Attardi LD, Auberger P, Auburger G, Aurelian L, Autelli R, Avagliano L, Avantaggiati ML, Avrahami L, Awale S, Azad N, Bachetti T, Backer JM, Bae DH, Bae JS, Bae ON, Bae SH, Baehrecke EH, Baek SH, Baghdiguian S, and Bagniewska-Zadworna A, et al. Guidelines for the use and interpretation of assays for monitoring autophagy (3rd edition). *AUTOPHAGY* 12: 1-222, 2016.

23. Klionsky DJ, Codogno P, Cuervo AM, Deretic V, Elazar Z, Fueyo-Margareto J, Gewirtz DA, Kroemer G, Levine B, Mizushima N, Rubinsztein DC, Thumm M, and Tooze SA. A comprehensive glossary of autophagy-related molecules and processes. *AUTOPHAGY* 6: 438-448, 2010.
24. Lepine S, Allegood JC, Park M, Dent P, Milstien S, and Spiegel S. Sphingosine-1-phosphate phosphohydrolase-1 regulates ER stress-induced autophagy. *CELL DEATH DIFFER* 18: 350-361, 2011.
25. Li C, Meng L, Li X, Li D, and Jiang LH. Non-NMDAR neuronal Ca(2+)-permeable channels in delayed neuronal death and as potential therapeutic targets for ischemic brain damage. *Expert Opin Ther Targets* 19: 879-892, 2015.
26. Li X, Tao RR, Hong LJ, Cheng J, Jiang Q, Lu YM, Liao MH, Ye WF, Lu NN, Han F, Hu YZ, and Hu YH. Visualizing peroxynitrite fluxes in endothelial cells reveals the dynamic progression of brain vascular injury. *J AM CHEM SOC* 137: 12296-12303, 2015.
27. Lindahl P, Johansson BR, Leveen P, and Betsholtz C. Pericyte loss and microaneurysm formation in PDGF-B-deficient mice. *SCIENCE* 277: 242-245, 1997.
28. Liu B, Tewari AK, Zhang L, Green-Church KB, Zweier JL, Chen YR, and He G. Proteomic analysis of protein tyrosine nitration after ischemia reperfusion injury: mitochondria as the major target. *Biochim Biophys Acta* 1794: 476-485, 2009.
29. Lu YM, Gao YP, Tao RR, Liao MH, Huang JY, Wu G, Han F, and Li XM. Calpain-Dependent ErbB4 Cleavage Is Involved in Brain Ischemia-Induced Neuronal Death. *MOL NEUROBIOL* 53: 2600-2609, 2016.
30. Lu YM, Huang J, Shioda N, Fukunaga K, Shirasaki Y, Li XM, and Han F. CaMKIIdeltaB mediates aberrant NCX1 expression and the imbalance of NCX1/SERCA in transverse aortic constriction-induced failing heart. *PLOS ONE* 6: e24724, 2011.
31. Luan Q, Jin L, Jiang CC, Tay KH, Lai F, Liu XY, Liu YL, Guo ST, Li CY, Yan XG, Tseng HY, and Zhang XD. RIPK1 regulates survival of human melanoma cells upon endoplasmic reticulum stress through autophagy. *AUTOPHAGY* 11: 975-994, 2015.
32. Mei ZZ, Xia R, Beech DJ, and Jiang LH. Intracellular coiled-coil domain engaged in subunit interaction and assembly of melastatin-related transient receptor potential channel 2. *J BIOL CHEM* 281: 38748-38756, 2006.

33. Mizushima N, Yoshimori T and Levine B. Methods in mammalian autophagy research. *CELL* 140: 313-326, 2010.
34. Muller C, Salvayre R, Negre-Salvayre A, and Vindis C. Oxidized LDLs trigger endoplasmic reticulum stress and autophagy: prevention by HDLs. *AUTOPHAGY* 7: 541-543, 2011.
35. Nakagawa S, Deli MA, Nakao S, Honda M, Hayashi K, Nakaoke R, Kataoka Y, and Niwa M. Pericytes from brain microvessels strengthen the barrier integrity in primary cultures of rat brain endothelial cells. *CELL MOL NEUROBIOL* 27: 687-694, 2007.
36. Ng S, Wu YT, Chen B, Zhou J, and Shen HM. Impaired autophagy due to constitutive mTOR activation sensitizes TSC2-null cells to cell death under stress. *AUTOPHAGY* 7: 1173-1186, 2011.
37. Niu F, Yao H, Zhang W, Sutliff RL, and Buch S. Tat 101-mediated enhancement of brain pericyte migration involves platelet-derived growth factor subunit B homodimer: implications for human immunodeficiency virus-associated neurocognitive disorders. *J NEUROSCI* 34: 11812-11825, 2014.
38. Qin L, Wang Z, Tao L, and Wang Y. ER stress negatively regulates AKT/TSC/mTOR pathway to enhance autophagy. *AUTOPHAGY* 6: 239-247, 2010.
39. Roy R, Singh SK, Chauhan LK, Das M, Tripathi A, and Dwivedi PD. Zinc oxide nanoparticles induce apoptosis by enhancement of autophagy via PI3K/Akt/mTOR inhibition. *TOXICOL LETT* 227: 29-40, 2014.
40. Sagare AP, Bell RD, Zhao Z, Ma Q, Winkler EA, Ramanathan A, and Zlokovic BV. Pericyte loss influences Alzheimer-like neurodegeneration in mice. *NAT COMMUN* 4: 2932, 2013.
41. Sava P, Cook IO, Mahal RS, and Gonzalez AL. Human microvascular pericyte basement membrane remodeling regulates neutrophil recruitment. *MICROCIRCULATION* 22: 54-67, 2015.
42. Sheng R, Liu XQ, Zhang LS, Gao B, Han R, Wu YQ, Zhang XY, and Qin ZH. Autophagy regulates endoplasmic reticulum stress in ischemic preconditioning. *AUTOPHAGY* 8: 310-325, 2012.
43. Syed MS, Wang L, Li D, and Jiang LH. TRPM2 Channel-Mediated ROS-Sensitive Ca(2+) Signaling Mechanisms in Immune Cells. *Front Immunol* 6: 407, 2015.
44. Szabo C, Ischiropoulos H and Radi R. Peroxynitrite: biochemistry, pathophysiology and development of therapeutics. *NAT REV DRUG DISCOV* 6: 662-680, 2007.
45. Tan SH, Shui G, Zhou J, Shi Y, Huang J, Xia D, Wenk MR, and Shen HM. Critical role of SCD1 in autophagy regulation via lipogenesis and lipid rafts-coupled AKT-FOXO1 signaling pathway. *AUTOPHAGY* 10: 226-242, 2014.
46. Tao RR, Huang JY, Shao XJ, Ye WF, Tian Y, Liao MH, Fukunaga K, Lou YJ,

Han F, and Lu YM. Ischemic injury promotes Keap1 nitration and disturbance of antioxidative responses in endothelial cells: a potential vasoprotective effect of melatonin. *J PINEAL RES* 54: 271-281, 2013.

47. Tao RR, Ji YL, Lu YM, Fukunaga K, and Han F. Targeting nitrosative stress for neurovascular protection: new implications in brain diseases. *CURR DRUG TARGETS* 13: 272-284, 2012.
48. Tao RR, Wang H, Hong LJ, Huang JY, Lu YM, Liao MH, Ye WF, Lu NN, Zhu DY, Huang Q, Fukunaga K, Lou YJ, Shoji I, Wilcox CS, Lai EY, and Han F. Nitrosative stress induces peroxiredoxin 1 ubiquitination during ischemic insult via E6AP activation in endothelial cells both in vitro and in vivo. *Antioxid Redox Signal* 21: 1-16, 2014.
49. Winkler EA, Sagare AP and Zlokovic BV. The pericyte: a forgotten cell type with important implications for Alzheimer's disease? *BRAIN PATHOL* 24: 371-386, 2014.
50. Wong CH, Heit B and Kubes P. Molecular regulators of leucocyte chemotaxis during inflammation. *CARDIOVASC RES* 86: 183-191, 2010.
51. Yang W, Manna PT, Zou J, Luo J, Beech DJ, Sivaprasadarao A, and Jiang LH. Zinc inactivates melastatin transient receptor potential 2 channels via the outer pore. *J BIOL CHEM* 286: 23789-23798, 2011.
52. Yao Y, Chen ZL, Norris EH, and Strickland S. Astrocytic laminin regulates pericyte differentiation and maintains blood brain barrier integrity. *NAT COMMUN* 5: 3413, 2014.
53. Ye M, Yang W, Ainscough JF, Hu XP, Li X, Sedo A, Zhang XH, Zhang X, Chen Z, Li XM, Beech DJ, Sivaprasadarao A, Luo JH, and Jiang LH. TRPM2 channel deficiency prevents delayed cytosolic Zn2+ accumulation and CA1 pyramidal neuronal death after transient global ischemia. *CELL DEATH DIS* 5: e1541, 2014.
54. Yemisci M, Gursoy-Ozdemir Y, Vural A, Can A, Topalkara K, and Dalkara T. Pericyte contraction induced by oxidative-nitrative stress impairs capillary reflow despite successful opening of an occluded cerebral artery. *NAT MED* 15: 1031-1037, 2009.
55. Yu W, Jiang LH, Zheng Y, Hu X, Luo J, and Yang W. Inactivation of TRPM2 channels by extracellular divalent copper. *PLOS ONE* 9: e112071, 2014.
56. Zhang W, Chu X, Tong Q, Cheung JY, Conrad K, Masker K, and Miller BA. A novel TRPM2 isoform inhibits calcium influx and susceptibility to cell death. *J BIOL CHEM* 278: 16222-16229, 2003.
57. Zhang X, Yuan Y, Jiang L, Zhang J, Gao J, Shen Z, Zheng Y, Deng T, Yan H, Li W, Hou WW, Lu J, Shen Y, Dai H, Hu WW, Zhang Z, and Chen Z. Endoplasmic reticulum stress induced by tunicamycin and thapsigargin protects against transient ischemic brain injury: Involvement of PARK2-dependent mitophagy. *AUTOPHAGY* 10: 1801-1813, 2014.
58. Zou J, Ainscough JF, Yang W, Sedo A, Yu SP, Mei ZZ, Sivaprasadarao A,

Beech DJ, and Jiang LH. A differential role of macrophage TRPM2 channels in Ca(2)(+) signaling and cell death in early responses to H(2)O(2). *Am J Physiol Cell Physiol* 305: C61-C69, 2013.

Figure legends

Figure 1. Changes in autophagy-lysosome signaling during pericyte injury.

(A) Representative western blots showing the changes of LC3-I and LC3-II in pericytes after treatments with indicated concentrations of ZnO-NP for 6 h. **(B)** Quantitative analyses of results, as shown in (**A**), and presented the bar graph as the densitometry ratio of control, from 3 independent experiments. $^{**}P < 0.01$, $^{***}P < 0.001$ versus control. **(C)** Representative electron microscopic images showing autophagy vacuoles in control pericytes and cells treated with 10 μg/ml ZnO-NP for 6 h. Double arrows, autophagosome; single arrow, lysosome. **(D)** Representative confocal microscopic images showing LC3 puncta in cells under indicated conditions. The autophagy flux was examined in cells after ZnO-NP exposure for 6 h. **(E)** The average number of LC3 puncta per cell in control cells and cells treated with ZnO-NP. n = 37 cells analyzed for each condition. $^{***}P < 0.001$ versus control. **(F)** Representative images at indicated time points of pericytes transfected with mRFP-GFP-LC3 without (control, upper panel) or with exposure to 15 μg/ml ZnO-NP (bottom panel) for 60 min. The inserts showing magnified images of GFP-LC3 and mRFP-LC3 puncta. **(G)** ZnO-NP induced autophagy by enhancing autophagosome formation. ZnO-NP treatment increased the relative level of LC3-II and Bafilomycin A1 (Baf-A1) caused a further increase. The inserts showing magnified images of GFP-LC3 and mRFP-LC3 puncta. **(H)** The average number of GFP-LC3 or RFP-LC3 puncta per cell in control cells and ZnO-NP-treated cells. n = 27 cells analyzed for each condition. $^{***}P < 0.001$ versus control; $^{\#\#\#}P < 0.001$ versus ZnO-NP treatment alone.

Figure 2. TRPM2 knockdown blocks disturbance of autophagy flux during pericyte injury.

(A) Representative western blots showing the change in TRPM2 protein levels in

pericytes after treatment with 10 μg/ml ZnO-NP for indicated durations. Note that an increase in the expression of TRPM2-S revealed upon short exposure. **(B)** Quantitative analyses of the resultsas shown in (**A**) and presented in the bar graph as the densitometry ratio of the control from 3 independent experiments. $^{*}P < 0.05$, and $^{***}P < 0.001$ versus control. **(C)** Representative western blot showing ZnO-NP-induced LC3-II accumulation in control pericytes or cells transfected with scramble-siRNA (siScramble) or TRPM2-siRNA (siTRPM2). Cells were exposed to 10 μg/ml ZnO-NP for 6 h. **(D)** Quantitative analyses of the results, as shown in **(C)**, and presented in the bar graph as the densitometry ratio of the control from 3 independent experiments. $^{***}P < 0.001$ versus control; $^{###}P<0.001$ versus ZnO-NP treatment alone. **(E)** Representative western blot showing ZnO-NP-induced LC3-II accumulation in pericytes treated with indicated conditions. Cells were exposed to ZnO-NP or chloroquine for indicated time. **(F)** Quantitative analyses of the result as shown in **(E)** and presented in the bar graph as the densitometry ratio of the control from 3 independent experiments. $^{*}P < 0.05$, $^{**}P < 0.01$ and $^{***}P < 0.001$ versus control; $^{##}P < 0.01$ when compared with the indicated group.

Figure 3. TRPM2 knockdown reduces apoptosis and ER stress during pericyte injury.

(**A**) Representative images showing TUNEL (green) and DAPI staining (blue) in pericytes under indicated conditions. Pericytes were transfected with TRPM2 siRNA (siTRPM2) and then treated with 10 μg/ml ZnO-NP for 6 h. (**B**) Mean percentage of TUNEL positive pericytes under indicated conditions from 4 independent experiments. $^{***}P < 0.001$ versus ZnO-NP treatment alone, using unpaired Student's *t*-test. **(C)** Representative western blot showing ZnO-NP-induced ER stress signaling in control pericytes or cells transfected with scramble-siRNA (siScramble) or TRPM2-siRNA (siTRPM2). Cells were exposed to 10 μg/ml ZnO-NP for 6 h. Densitometry of phospho-JNK (**D**), phospho-PERK (**E**) and CHOP (**F**) levels in cells under indicated

conditions. Cells were treated with 10 μg/ml ZnO-NP for 6 h. $^{***}P < 0.001$ versus control; $^{###}P < 0.001$ versus ZnO-NP treatment alone. **(G)** Representative western blot showing ZnO-NP-induced ER stress signaling in pericytes treated with indicated conditions. Cells were exposed to ZnO-NP or chloroquine for indicated time. TRPM2-dependent ER stress-autophagy axis disturbance associates with ZnO-NP-induced pericyte injury. **(H)** Representative western blot showing TRPM2 knockdown reduced pericyte injury following treatment with 10 μg/ml ZnO-NP for 24 h.

Figure 4. ATG5 knockdown reduces ZnO-NP-induced apoptosis.

(**A**) Representative images showing double staining with TUNEL (green) and DAPI (blue) in pericytes after treatment with ZnO-NP (10 μg/ml) for 6 h. (**B**) Mean percentage of TNUL positive pericytes under indicated conditions from 3 independent experiments. $^{***}P < 0.001$ versus ZnO-NP treatment alone, using unpaired Student's *t*-test. Apoptosis was dramatically reduced following transfection with ATG5 siRNA (siATG5) in cells after ZnO-NP treatment. (**C**) Summary of the mean cell viability under indicated conditions determined in CCK8 assays from 4 independent experiments. The effect of Z-VAD-FMK, a caspase inhibitor, on cell viability also examined. $^{***}P < 0.001$ versus control; $^{###}P < 0.001$ versus ZnO-NP treatment alone. (**D**) Representative western blot showing ZnO-NP-induced caspase-8 cleavage and LC3-II accumulation in control pericytes or cells transfected with ATG5-siRNA (siATG5). Cells were exposed to 10 μg/ml ZnO-NP for 6 h. (**E**) Quantitative analyses of the results as shown in **(D)** and presented in the bar graph, from 3 independent experiments. $^{**}P < 0.01$ versus control; $^{##}P < 0.01$ versus ZnO-NP treatment alone. Ctrl, control. Error bars represent mean ± S.E.M.. (**F**) Relative caspase-8 activity as measured by optical density (O.D.) at 405 nm in control pericytes or cells transfected with scramble-siRNA (siScramble), TRPM2-siRNA (siTRPM2) and ATG5-siRNA (siATG5). Cells were exposed to 10 μg/ml ZnO-NP for 6 h. Data were from 3

independent experiments. $^{***}P < 0.001$ versus control; $^{\#\#\#}P < 0.001$ versus ZnO-NP treatment alone. (**G**) Representative flow cytometric dot plots of apoptotic cells under indicated conditions after ZnO-NP treatment with or without transfection. Pericytes were treated with ZnO-NP for 6 h after transfection with siRNA for TRPM2 or ATG5. Cells were stained with PI and analyzed by FACS. (**H**) Quantitative analyses of the results as shown in **(G)** and presented in the bar graph, from 3 independent experiments. $^{***}P < 0.001$ versus control; $^{\#}P < 0.05$; $^{\#\#}P < 0.01$ versus ZnO-NP treatment alone.

Figure 5. Nitrosative stress associates with autophagy during pericyte injury.

(A) Representative western blot showing temporal changes in peroxynitrite production in pericytes after treatment with 10 μg/ml ZnO-NP (6 h) for indicated durations. (**B**) Representative confocal images showing peroxynitrite production under indicated conditions. Measurement using NP3 of $ONOO^-$ formation in pericytes upon ZnO-NP treatment. Treatment with 200 μM UA, an $ONOO^-$ scavenger, reduced ZnO-NP-induced increase in NP3 fluorescence. Data were representatives of 3 independent experiments. (**C**) Representative confocal images showing effects of 200 μM UA on autophagic flux in pericytes following treatment with 10 μg/ml ZnO-NP. The inserts showing magnified images of GFP-LC3 and mRFP-LC3 puncta. (**D**) Inhibition of nitrosative stress-induced TRPM2-S formation and LC3-II formation. ZnO-NP induced an elevation in the TRPM2-S (**E**), which was attenuated by treatment with 100 μM L-NA and 200 μM UA. UA, uric acid; L-NA, L-NAME; L+U, L-NAME and uric acid. (**F**) Densitometric analysis of LC3B-II, normalized to β-actin (ACTB). Data shown in **(E)** and **(F)** were from 3 independent experiments. $^{**}P < 0.01$, $^{***}P < 0.001$ versus control; $^{\#\#}P < 0.01$, $^{\#\#\#}P < 0.001$ versus ZnO-NP treatment alone. (**G**) Effects of nitrosative stress inhibition on ER-associated apoptosis proteins. ZnO-NP-induced increase in phospho-JNK (**H**) and CHOP (**I**) were attenuated by treatment with L-NAME or uric acid. The data are expressed as percentages of values

of the control. $^{***}P < 0.001$ versus control; $^{###}P < 0.001$ versus ZnO-NP treatment alone.

Figure 6. Tandem mass spectrum identification of the nitration residue in the TRPM2 protein.

The protein was digested with 20 ng/μl trypsin and subjected to Nano-LC/MS/MS analysis. The sequence-specific ions are labeled as y and b ions on the spectra. The peptide (1236-1503) was identified to be nitrated. The peptide contained 3-nitrotyrosine at Y1485. The fragmentation of ions showing the diagnostic mass shift of +45 Da is indicated.

Figure 7. TRPM2 Y1485S mutation reduces pericyte injury.

(A) A schematic showing the location of Y1485 in the C-terminus of the TRPM2 protein. **(B)** Pericytes expressing the TRPM2 Y1485S mutant exhibited lower ZnO-NP (10 μg/ml)-induced autophagy events and ER stress. Cells were transfected with the plasmid encoding the TRPM2 Y1485S mutant or an empty vector as negative control. Quantitative analysis of the protein levels for LC3-II formation (**C**), CHOP levels (**D**), phospho-JNK (**E**) and phospho-PERK (**F**) was performed by densitometry. The mean data, expressed as the densitometry ratio of the control, were from 3 independent experiments. $^{***}P < 0.001$ versus control; $^{##}P < 0.01$, $^{###}P < 0.001$ versus ZnO-NP treatment alone. **(G)** Expression of the TRPM2 Y1485S mutant reduced $ONOO^-$-induced ER stress and autophagy in pericytes. **(H-J)** Quantitative analysis of the protein levels for **(G)** was performed by densitometry, from 3 independent experiments. $^{***}P<0.001$ versus control; $^{##}P<0.01$, $^{###}P<0.001$ versus ZnO-NP treatment alone. Ctrl, control.

Figure 8. Nitrosative stress downregulates the TRPM2 channel function.

(A) Representative patch clamp recordings of ADPR-induced whole-cell currents in tetracycline-induced HEK-293 cells expressing hTRPM2. Cells were pretreated with

either 10 μg/ml ZnO-NP or 0.5 mM SIN-1. Currents were evoked by 0.5 mM ADPR contained in the pipette solution after obtaining the whole-cell (WC) configuration. Extracellular application of 10 μM N-(*p*-amylcinnamoyl) anthranilic acid (ACA) was gived at the end of the recording to block the TRPM2 channel currents. **(B)** The mean ADPR-induced current amplitude in cells treated with indicated conditions. n = 4 cells recorded for each condition. $^{*}P < 0.05$ versus control; $^{\#}P < 0.05$ versus ZnO-NP treatment alone.

Figure 9. Changes of α-SMA in microvessels in wild-type and TRPM2 KO mice during neurovascular injury.

(A) Fluorescent immunohistochemical staining of α-SMA and laminin in the microvessels after ZnO-NP injection in wild type (WT) and TRPM2 KO mice. Anti-laminin (red) and α-SMA (green) staining were performed at 24 h after ZnO-NP injection. **(B)** ZnO-NP injection lead to an increase in the number of the disconnected patchy parts of α-SMA-positive cells in the WT mice, which was attenuated in the TRPM2 KO mice. n = 4 mice for each condition. $^{***}P < 0.001$ versus WT; $^{\#\#}P < 0.01$ versus WT+ZnO-NP.

Figure 10. Aberrant autophagy signaling was associated with the pericyte injury.

(A) Visualization of the brain cortex of animals injected with adenovirus carrying mRFP-GFP-LC3 treated or not with ZnO-NP (left panel). The pericytes were stained with anti-α-SMA antibody (pink). Scale bar, 10 μm. The insets of panels show high magnification Z-stack images of brain microvessel staining. **(B)** Quantification data shown that accumulation of mRFP-positive puncta was partially reduced in the vessels from the TRPM2 KO mice after neurovascular insult. n = 4 mice for each group.

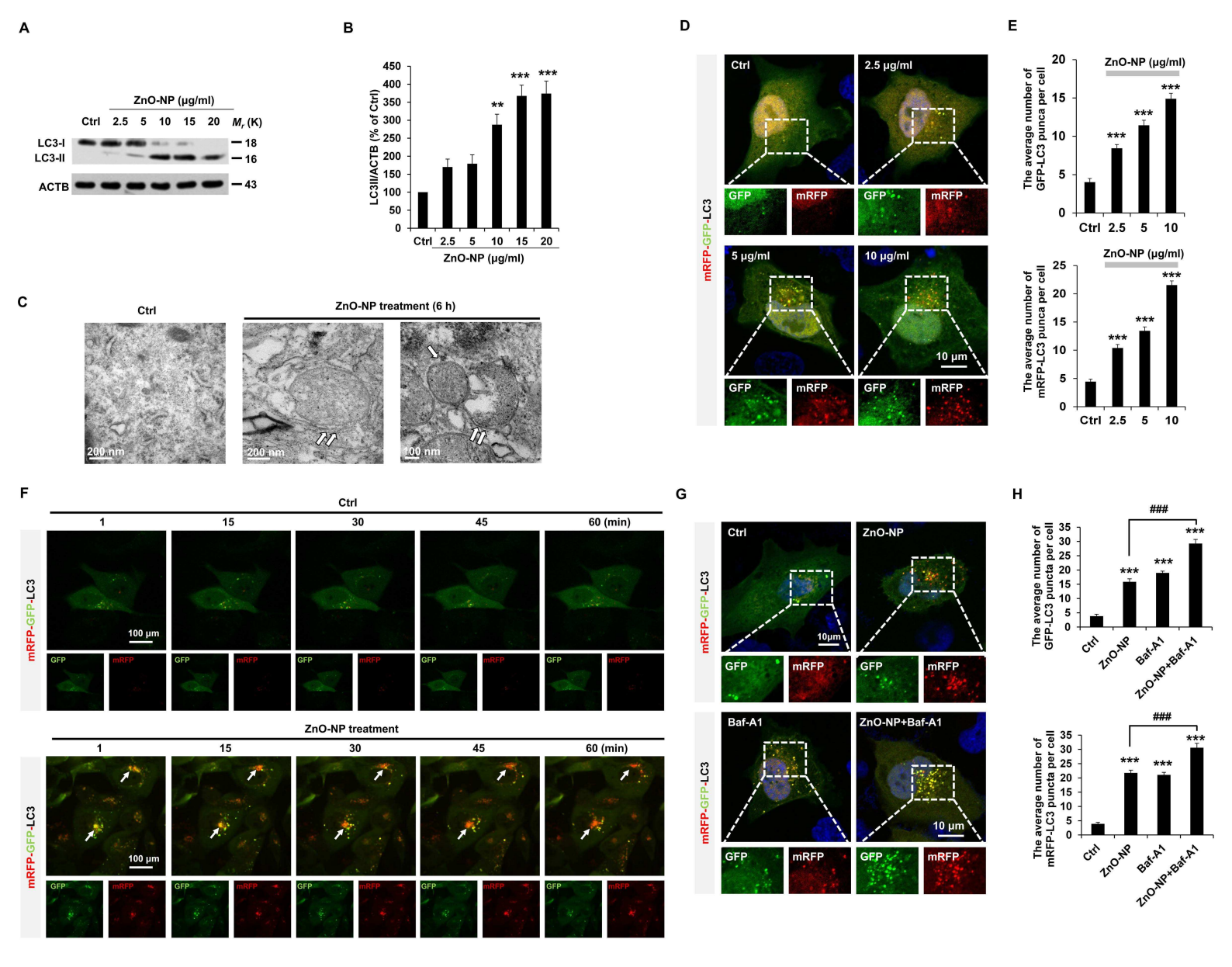
A
ZnO-NP (μg/ml)
Ctrl 2.5 5 10 15 20 M_r (K)
LC3-I
LC3-II
ACTB
18
16
43
B
LC3II/ACTB (% of Ctrl)
ZnO-NP (μg/ml)
C
Ctrl
ZnO-NP treatment (6 h)
200 nm
200 nm
100 nm
D
Ctrl
2.5 μg/ml
5 μg/ml
10 μg/ml
mRFP-GFP-LC3
GFP
mRFP
10 μm
E
The average number of GFP-LC3 punca per cell
The average number of mRFP-LC3 punca per cell
ZnO-NP (μg/ml)
F
Ctrl
ZnO-NP treatment
1 15 30 45 60 (min)
mRFP-GFP-LC3
100 μm
G
Ctrl
ZnO-NP
Baf-A1
ZnO-NP+Baf-A1
10μm
H
###
Ctrl
ZnO-NP
Baf-A1
ZnO-NP+Baf-A1

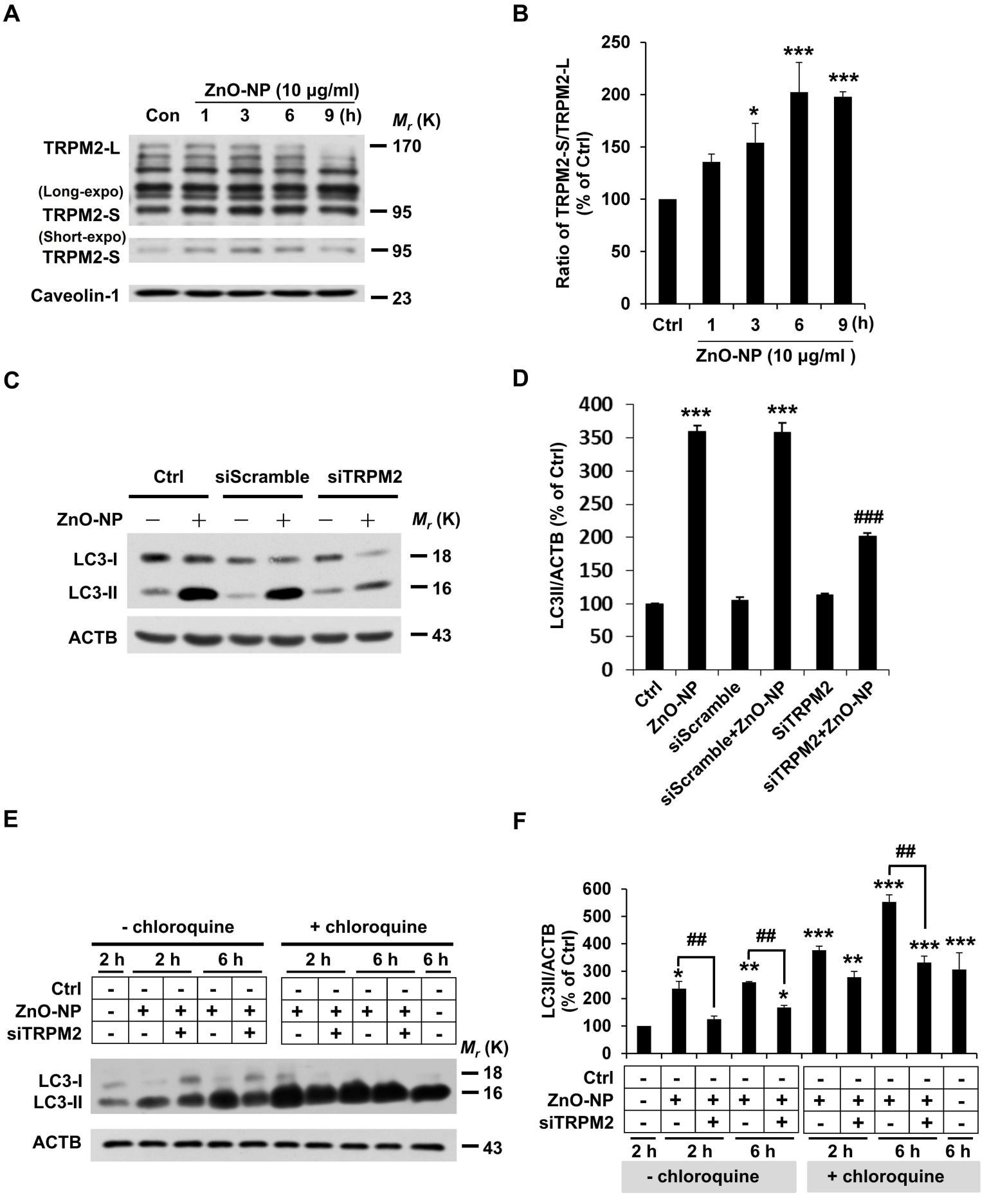
A
ZnO-NP (10 μg/ml)
Con
1
3
6
9 (h)
M_r (K)
TRPM2-L
(Long-expo)
TRPM2-S
(Short-expo)
TRPM2-S
Caveolin-1
170
95
95
23
B
Ratio of TRPM2-S/TRPM2-L (% of Ctrl)
250
200
150
100
50
0
***
*
***
Ctrl
1
3
6
9 (h)
ZnO-NP (10 μg/ml)
C
Ctrl
siScramble
siTRPM2
ZnO-NP
−
+
−
+
−
+
M_r (K)
LC3-I
LC3-II
ACTB
18
16
43
D
LC3II/ACTB (% of Ctrl)
400
350
300
250
200
150
100
50
0
***
***
###
Ctrl
ZnO-NP
siScramble
siScramble+ZnO-NP
SiTRPM2
siTRPM2+ZnO-NP
E
- chloroquine
+ chloroquine
2 h
2 h
6 h
2 h
6 h
6 h
Ctrl
ZnO-NP
siTRPM2
M_r (K)
LC3-I
LC3-II
ACTB
18
16
43
F
LC3II/ACTB (% of Ctrl)
600
500
400
300
200
100
0
##
##
##
*
**
*
***
**
***
***
***
Ctrl
ZnO-NP
siTRPM2
2 h
2 h
6 h
2 h
6 h
6 h
- chloroquine
+ chloroquine

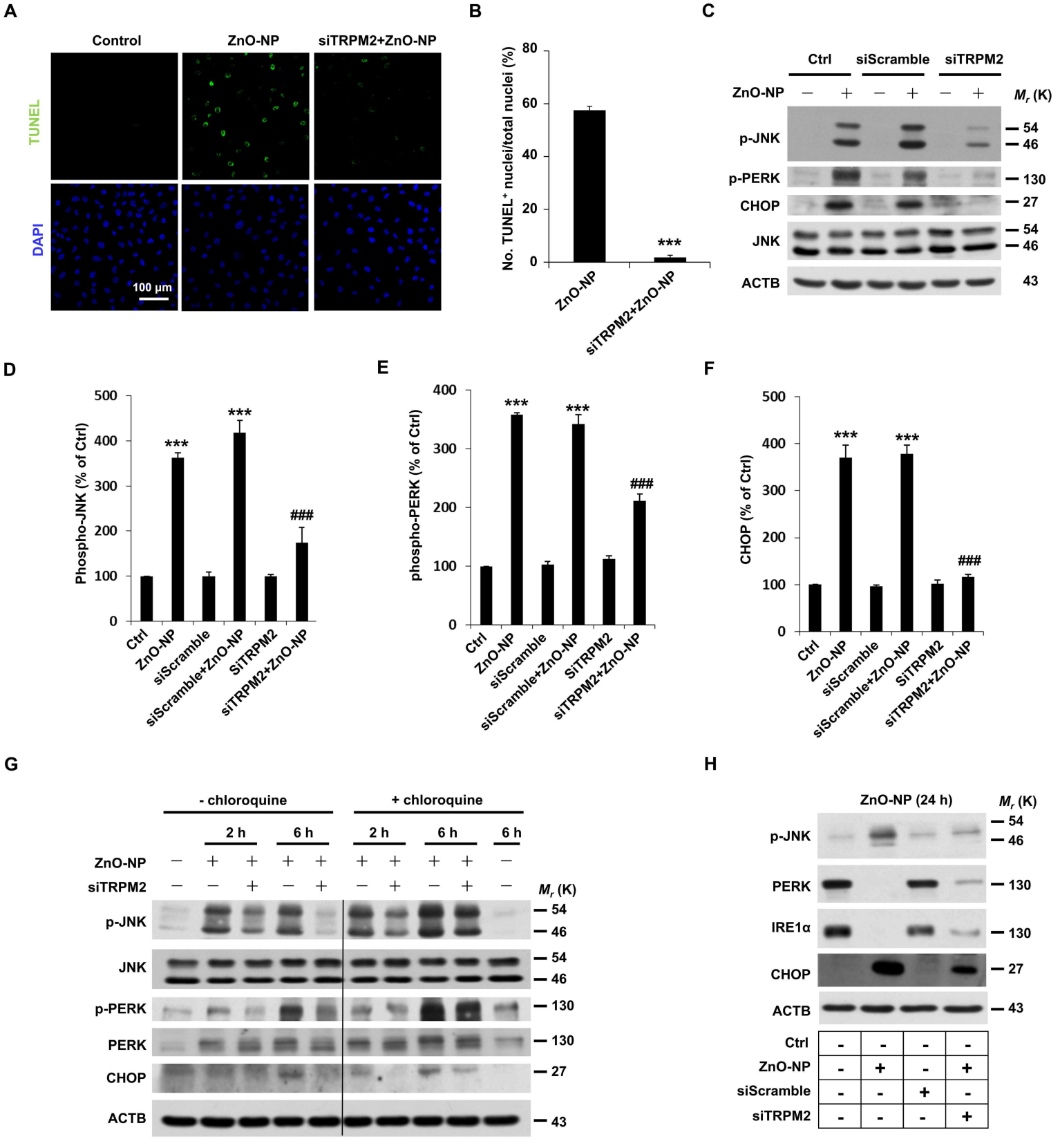
A
Control
ZnO-NP
siTRPM2+ZnO-NP
TUNEL
DAPI
100 μm
B
No. TUNEL+ nuclei/total nuclei (%)
80
60
40
20
0
***
ZnO-NP
siTRPM2+ZnO-NP
C
Ctrl
siScramble
siTRPM2
ZnO-NP
Mr (K)
p-JNK
54
46
p-PERK
130
CHOP
27
JNK
54
46
ACTB
43
D
Phospho-JNK (% of Ctrl)
500
400
300
200
100
0
***
***
###
Ctrl
ZnO-NP
siScramble
siScramble+ZnO-NP
SiTRPM2
siTRPM2+ZnO-NP
E
phospho-PERK (% of Ctrl)
400
300
200
100
0
***
***
###
Ctrl
ZnO-NP
siScramble
siScramble+ZnO-NP
SiTRPM2
siTRPM2+ZnO-NP
F
CHOP (% of Ctrl)
500
400
300
200
100
0
***
***
###
Ctrl
ZnO-NP
siScramble
siScramble+ZnO-NP
SiTRPM2
siTRPM2+ZnO-NP
G
- chloroquine
+ chloroquine
2 h
6 h
2 h
6 h
6 h
ZnO-NP
siTRPM2
Mr (K)
p-JNK
54
46
JNK
54
46
p-PERK
130
PERK
130
CHOP
27
ACTB
43
H
ZnO-NP (24 h)
Mr (K)
p-JNK
54
46
PERK
130
IRE1α
130
CHOP
27
ACTB
43
Ctrl
ZnO-NP
siScramble
siTRPM2

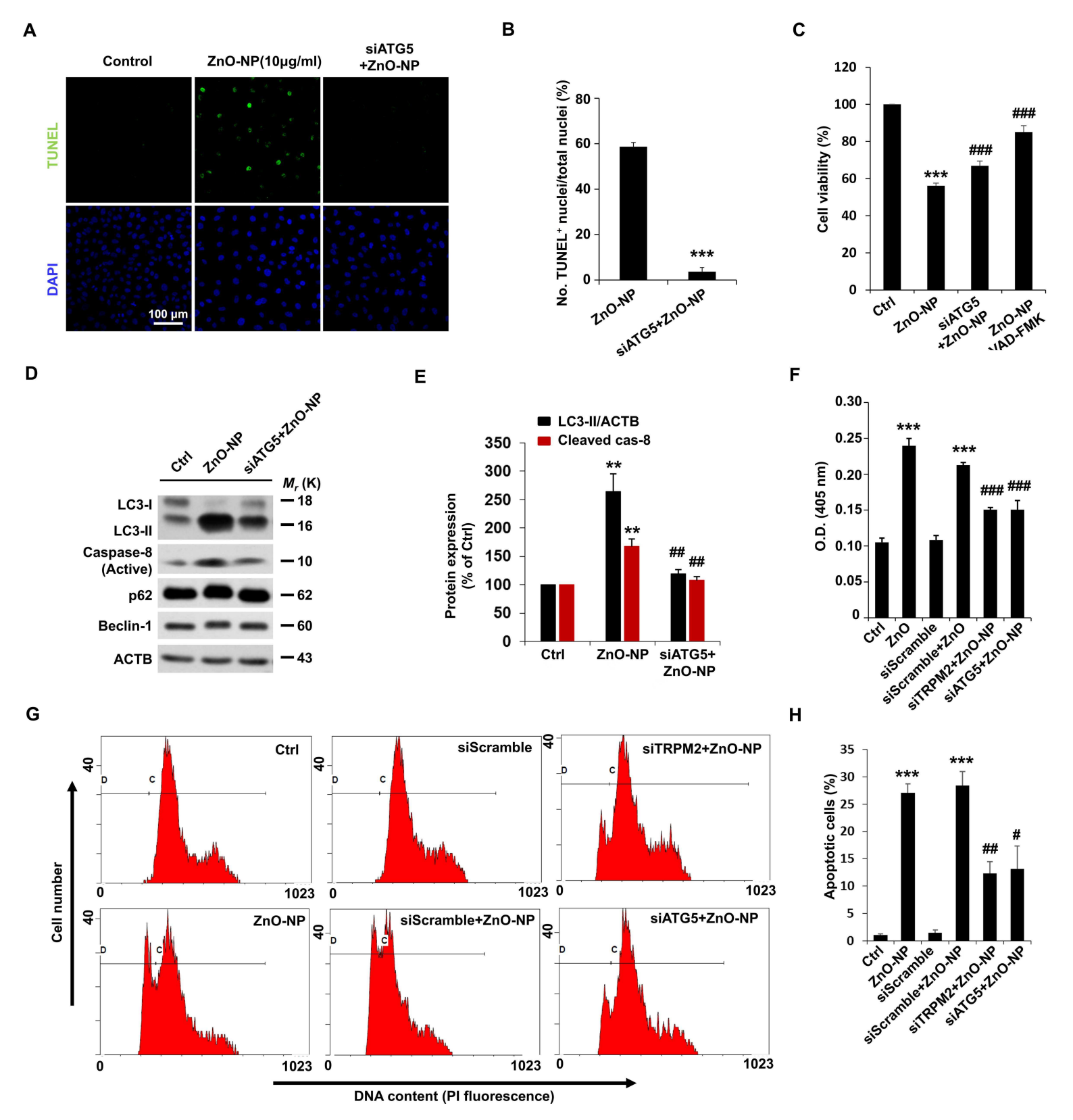
A
Control
ZnO-NP(10μg/ml)
siATG5 +ZnO-NP
TUNEL
DAPI
100 μm
B
No. TUNEL+ nuclei/total nuclei (%)
ZnO-NP
siATG5+ZnO-NP
C
Cell viability (%)
Ctrl
ZnO-NP
siATG5 +ZnO-NP
ZnO-NP +Z-VAD-FMK
D
Ctrl
ZnO-NP
siATG5+ZnO-NP
Mr (K)
LC3-I
LC3-II
Caspase-8 (Active)
p62
Beclin-1
ACTB
E
LC3-II/ACTB
Cleaved cas-8
Protein expression (% of Ctrl)
Ctrl
ZnO-NP
siATG5+ ZnO-NP
F
O.D. (405 nm)
Ctrl
ZnO
siScramble
siScramble+ZnO
siTRPM2+ZnO-NP
siATG5+ZnO-NP
G
Ctrl
siScramble
siTRPM2+ZnO-NP
ZnO-NP
siScramble+ZnO-NP
siATG5+ZnO-NP
Cell number
DNA content (PI fluorescence)
H
Apoptotic cells (%)
Ctrl
ZnO-NP
siScramble
siScramble+ZnO-NP
siTRPM2+ZnO-NP
siATG5+ZnO-NP

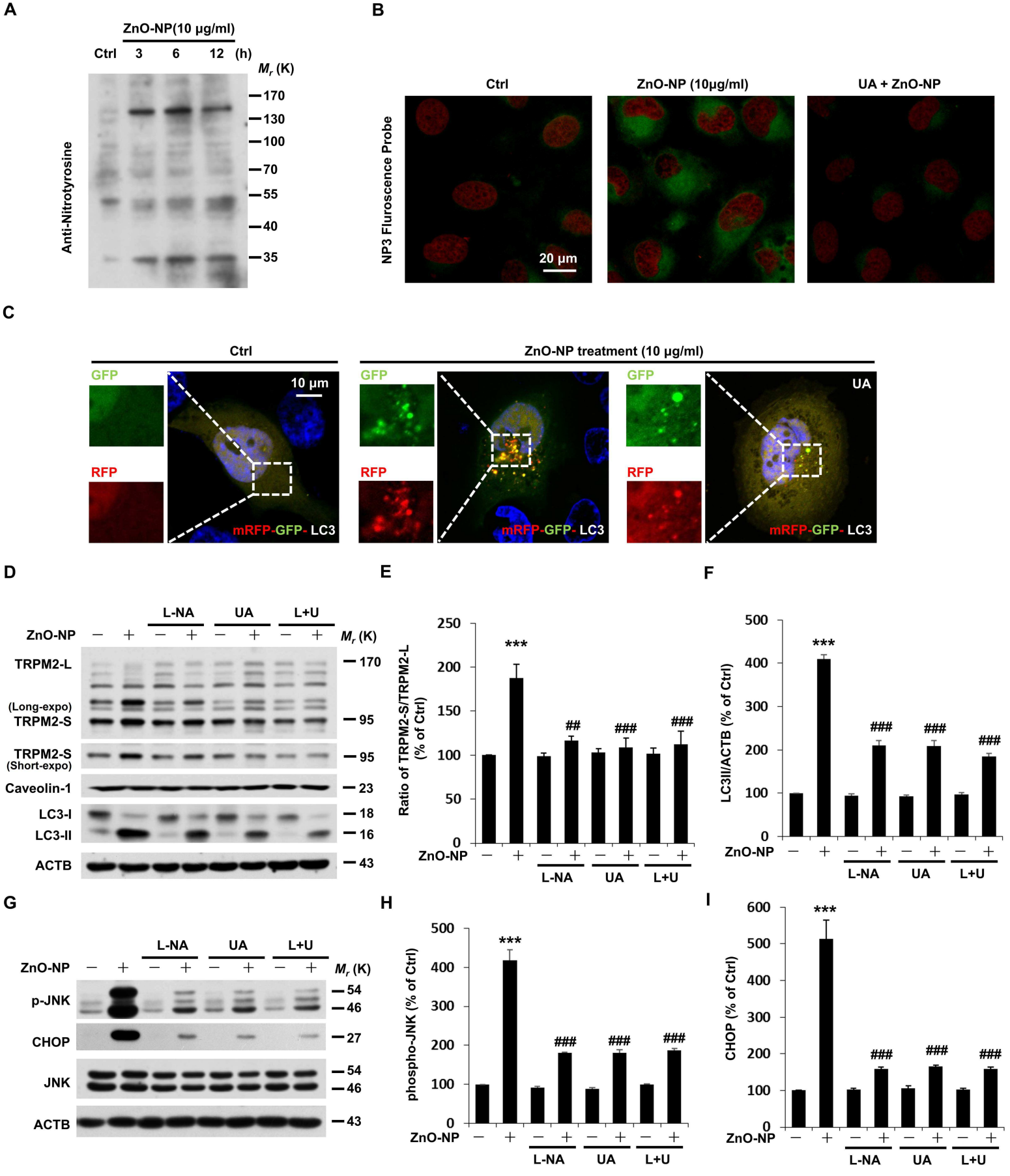
A
ZnO-NP(10 μg/ml)
Ctrl 3 6 12 (h)
M_r (K)
170
130
100
70
55
40
35
Anti-Nitrotyrosine
B
Ctrl
ZnO-NP (10μg/ml)
UA + ZnO-NP
NP3 Fluroscence Probe
20 μm
C
Ctrl
ZnO-NP treatment (10 μg/ml)
GFP
RFP
10 μm
mRFP-GFP- LC3
UA
D
L-NA
UA
L+U
ZnO-NP
M_r (K)
TRPM2-L
(Long-expo)
TRPM2-S
TRPM2-S
(Short-expo)
Caveolin-1
LC3-I
LC3-II
ACTB
170
95
95
23
18
16
43
E
Ratio of TRPM2-S/TRPM2-L
(% of Ctrl)
***
##
###
F
LC3II/ACTB (% of Ctrl)
G
p-JNK
CHOP
JNK
ACTB
54
46
27
54
46
43
H
phospho-JNK (% of Ctrl)
I
CHOP (% of Ctrl)

（FDSYHVNARHLLYPNCPVTRFPVPNEKVPWETEFLIYDPPFYTAERKDAAAMDPMGD
TLEPLSTIQYNVVDGLRDRRSFHGPYTVQAGLPLNPMGRTGLRGRGSLSCFGPNHTLYPM
[VTRWRRNEDGAICRKSIKKMLEVLVVKLPLSEHWALPGGSREPGEMLPRKLKRILRQEH
WPSFENLLKCGMEVYKGYMDDPRNTDNAWIETVAVSVHFQDQNDVELNRLNSNLHAC
DSGASIRWQVVDRRIPLYANHKTLLQKAAAE]FGAHY*）

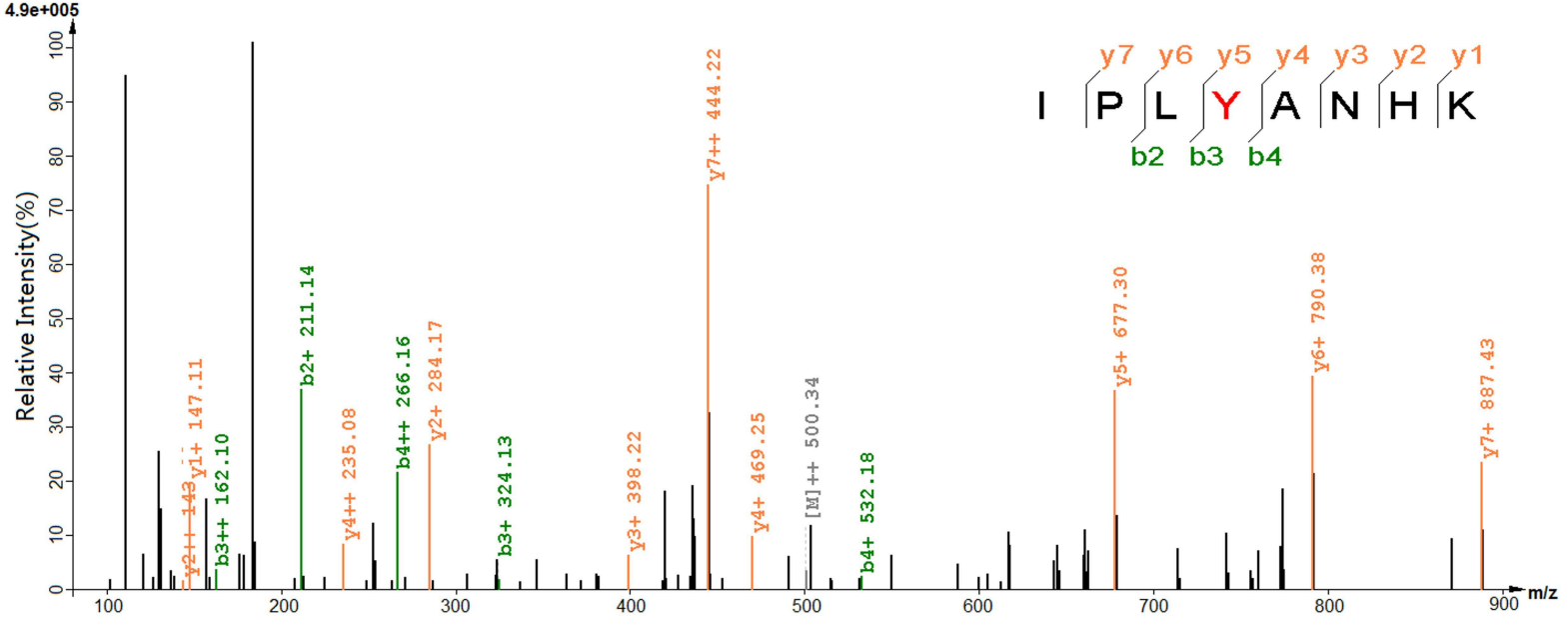

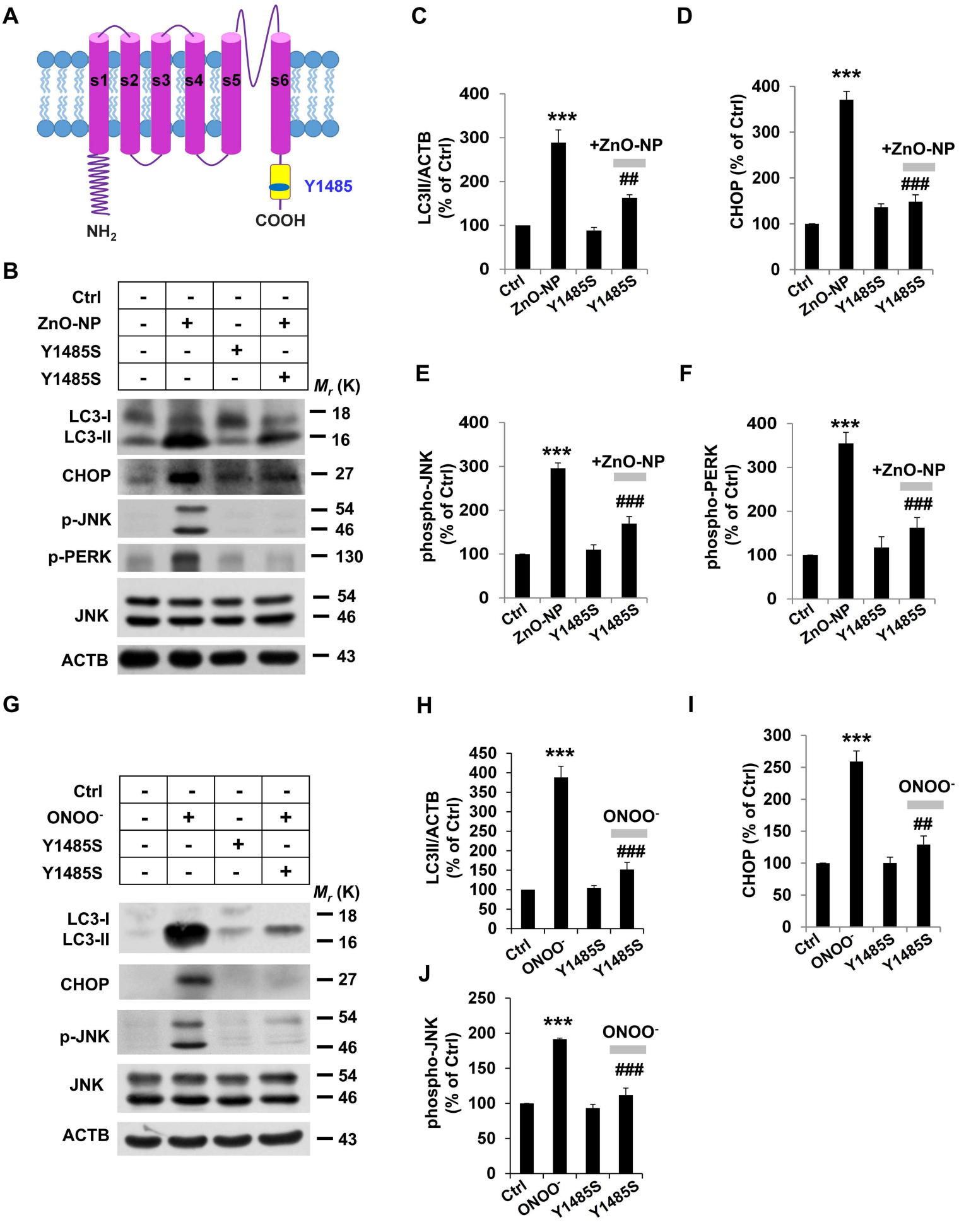
A
s1
s2
s3
s4
s5
s6
Y1485
COOH
NH2
B
Ctrl
ZnO-NP
Y1485S
Y1485S
Mr (K)
LC3-I
LC3-II
CHOP
p-JNK
p-PERK
JNK
ACTB
18
16
27
54
46
130
54
46
43
C
LC3II/ACTB (% of Ctrl)
+ZnO-NP
D
CHOP (% of Ctrl)
+ZnO-NP
E
phospho-JNK (% of Ctrl)
+ZnO-NP
F
phospho-PERK (% of Ctrl)
+ZnO-NP
G
Ctrl
ONOO-
Y1485S
Y1485S
Mr (K)
LC3-I
LC3-II
CHOP
p-JNK
JNK
ACTB
18
16
27
54
46
54
46
43
H
LC3II/ACTB (% of Ctrl)
ONOO-
I
CHOP (% of Ctrl)
ONOO-
J
phospho-JNK (% of Ctrl)
ONOO-
Ctrl
ZnO-NP
ONOO-
Y1485S

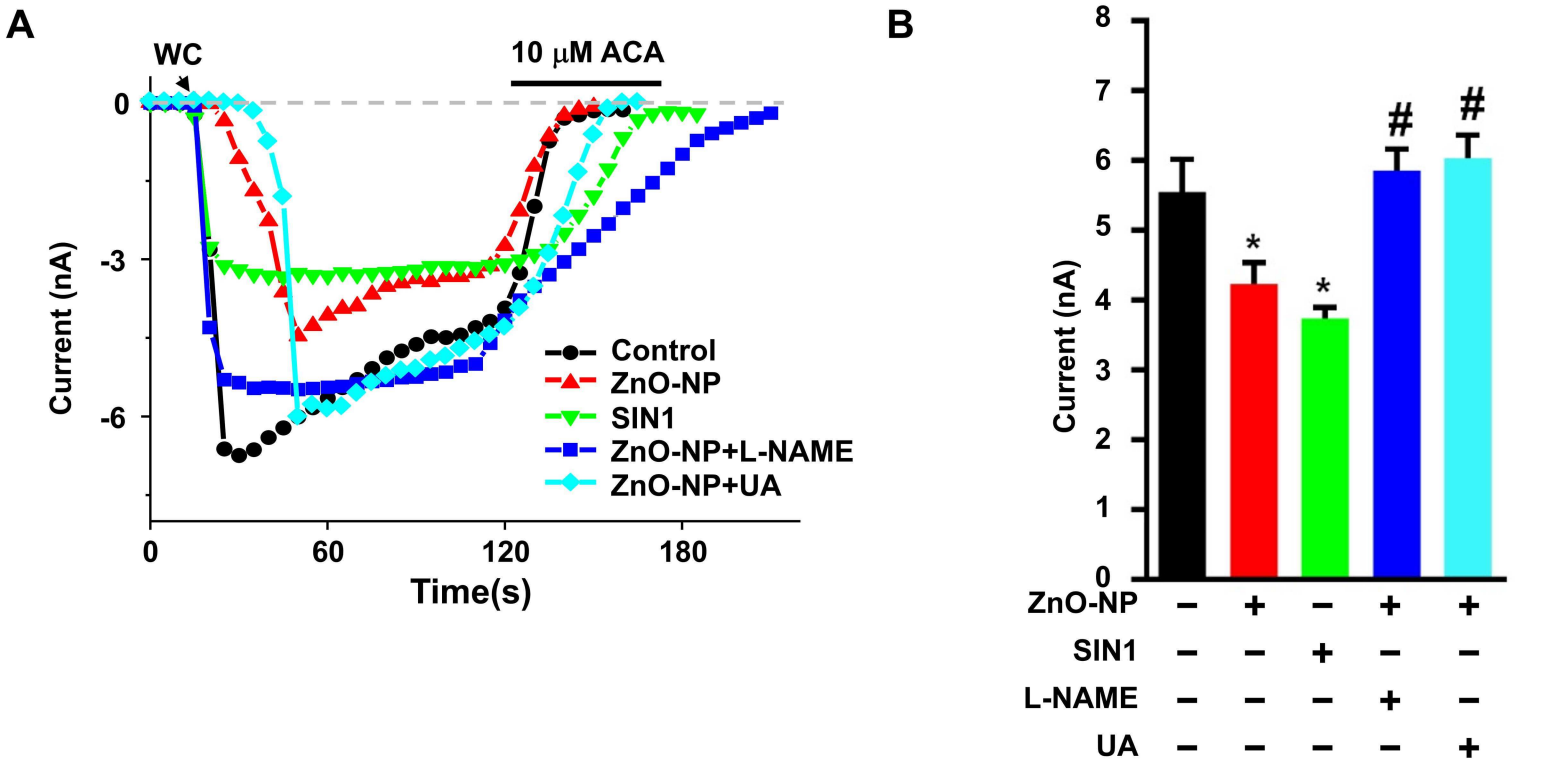
A
WC
10 μM ACA
0
-3
-6
Current (nA)
0
60
120
180
Time(s)
Control
ZnO-NP
SIN1
ZnO-NP+L-NAME
ZnO-NP+UA
B
Current (nA)
0
1
2
3
4
5
6
7
8
*
*
#
#
ZnO-NP – + – + +
SIN1 – – + – –
L-NAME – – – + –
UA – – – – +

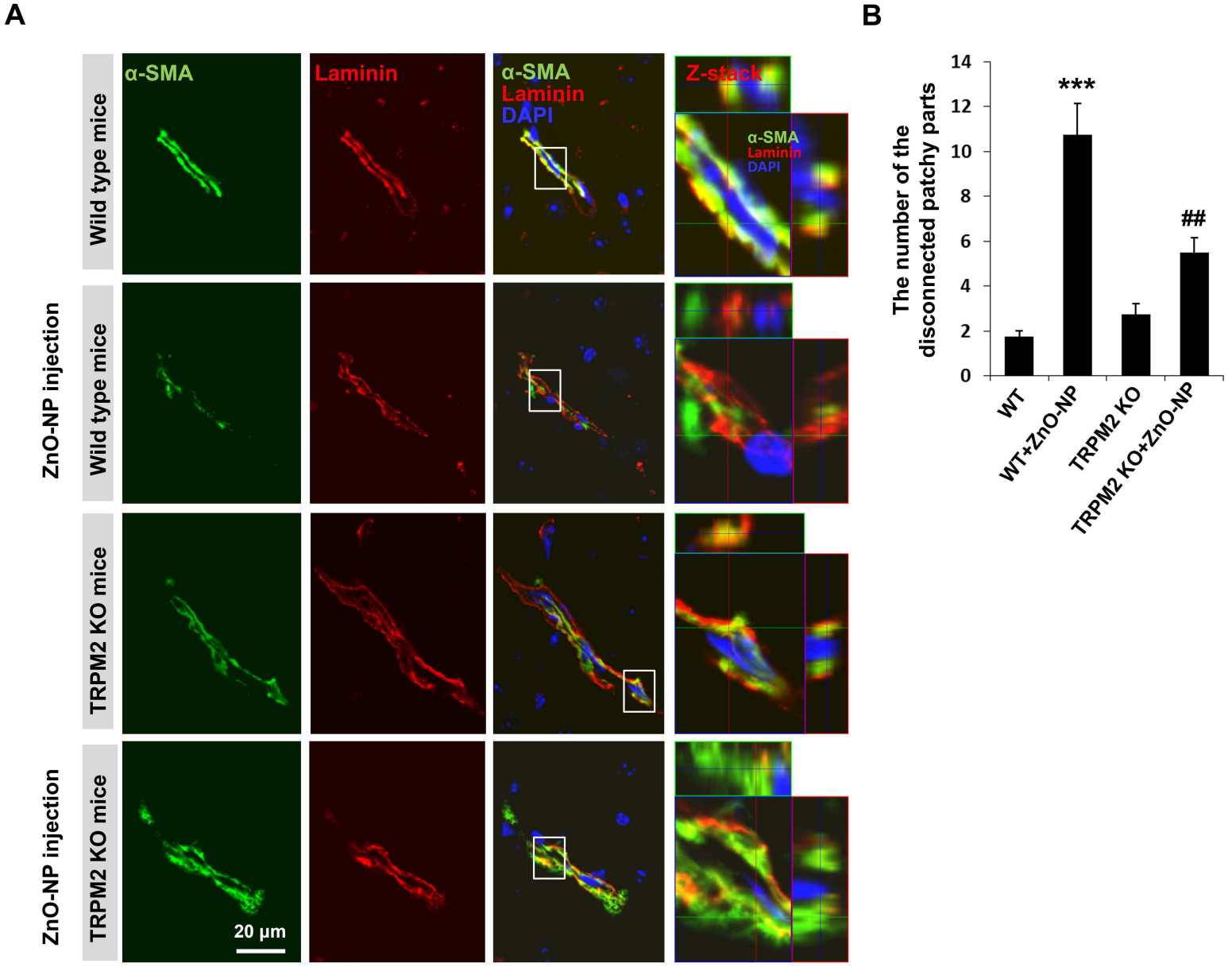
A
α-SMA
Laminin
α-SMA
Laminin
DAPI
Z-stack
α-SMA
Laminin
DAPI
Wild type mice
ZnO-NP injection
Wild type mice
TRPM2 KO mice
ZnO-NP injection
TRPM2 KO mice
20 μm
B
The number of the disconnected patchy parts
14
12
10
8
6
4
2
0
***
##
WT
WT+ZnO-NP
TRPM2 KO
TRPM2 KO+ZnO-NP

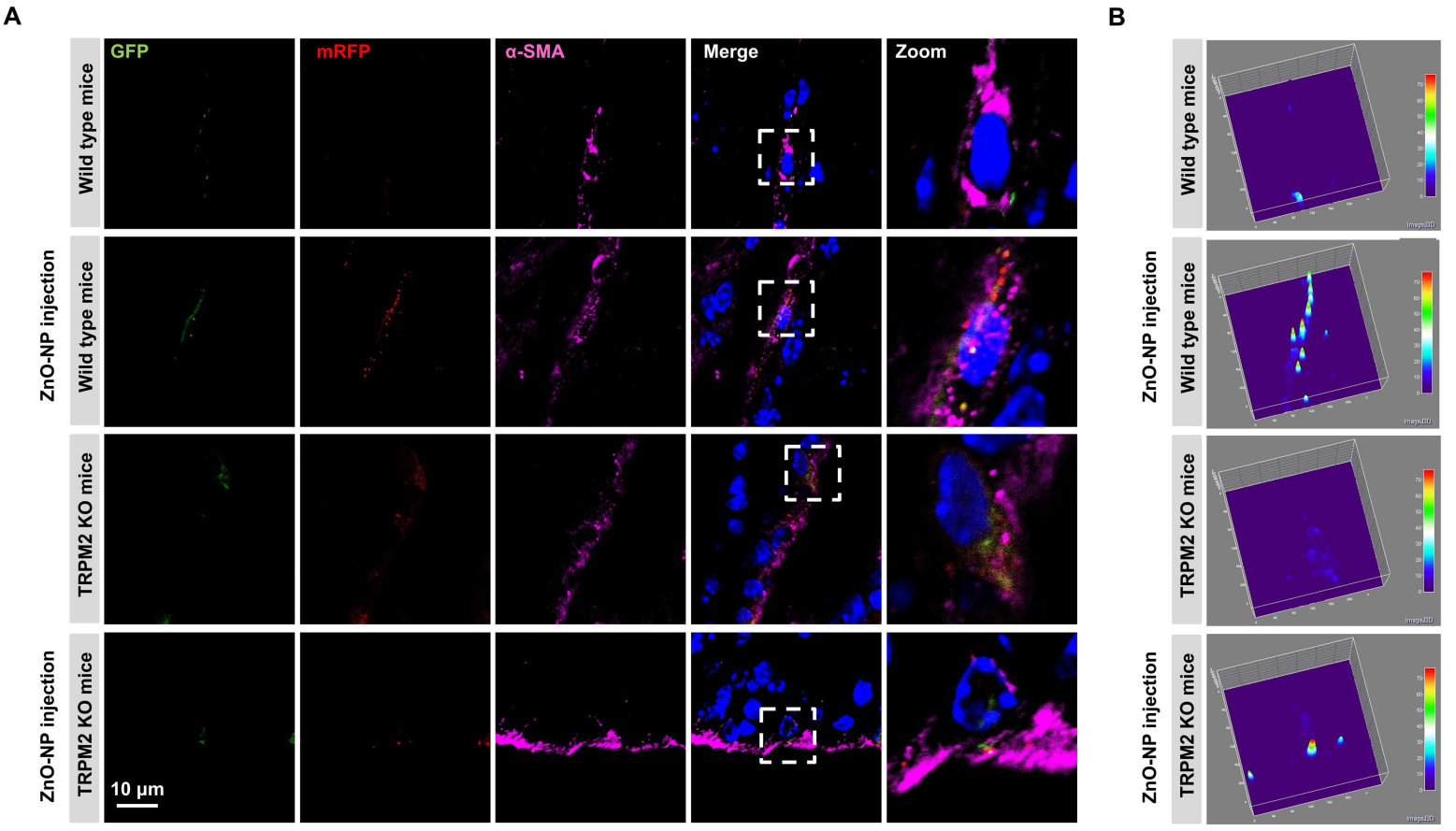
A
B
GFP
mRFP
α-SMA
Merge
Zoom
Wild type mice
ZnO-NP injection
Wild type mice
TRPM2 KO mice
ZnO-NP injection
TRPM2 KO mice
10 μm